Redox Regulation of Brain Selective Kinases BRSK1/2: Implications for Dynamic Control of the Eukaryotic AMPK family through Cys-based mechanisms

George N. Bendzunas [1#,] Dominic P Byrne [2#,] Safal Shrestha [3], Leonard A Daly [2,4], Sally O. Oswald [2,4], Samiksha Katiyar [1], Aarya Venkat [1], Wayland Yeung [1,3], Claire E Eyers [2,4], Patrick A Eyers* [3], Natarajan Kannan* [1,2]

# Equal contributions

[1] Department of Biochemistry and Molecular Biology, University of Georgia, Athens, GA 30602, USA [2] Department of Biochemistry, Cell and Systems Biology, Institute of Systems, Molecular and Integrative Biology, University of Liverpool, Liverpool L69 7ZB, UK. [3] Institute of Bioinformatics, University of Georgia, Athens, GA 30602, USA. [4] Centre for Proteome Research, Institute of Systems, Molecular and Integrative Biology, University of Liverpool, Liverpool L69 7ZB, UK

*Correspondence to: Natarajan Kannan, Email: nkannan@uga.edu or Patrick Eyers, Email: patrick.eyers@liverpool.ac.uk

Abstract

In eukaryotes, protein kinase signaling is regulated by a diverse array of post-translational modifications (PTMs), including phosphorylation of Ser/Thr residues and oxidation of cysteine (Cys) residues. While regulation by activation segment phosphorylation of Ser/Thr residues is well understood, relatively little is known about how oxidation of cysteine residues modulate catalysis. In this study, we investigate redox regulation of the AMPK-related Brain-selective kinases (BRSK) 1 and 2, and detail how broad catalytic activity is directly regulated through reversible oxidation and reduction of evolutionarily conserved Cys residues within the catalytic domain. We show that redox-dependent control of BRSKs is a dynamic and multilayered process involving oxidative modifications of several Cys residues, including the formation of intra-molecular disulfide bonds involving a pair of Cys residues near the catalytic HRD motif and a highly conserved T-Loop Cys with a BRSK-specific Cys within an unusual CPE motif at the end of the activation segment. Consistently, mutation of the CPE-Cys increases catalytic activity *in vitro* and drives phosphorylation of the BRSK substrate Tau in cells. Molecular modeling and molecular dynamics simulations indicate that oxidation of the CPE-Cys destabilizes a conserved salt bridge network critical for allosteric activation. The occurrence of spatially proximal Cys amino acids in diverse Ser/Thr protein kinase families suggests that disulfide mediated control of catalytic activity may be a prevalent mechanism for regulation within the broader AMPK family.

Introduction

Protein kinases are crucial components in cellular signaling networks, functioning as reversible molecular switches that orchestrate various biological processes. There are over 500 protein kinases encoded in the human genome that coordinate a wide range of cellular processes by catalyzing the transfer of a phosphate group from ATP to a hydroxyl group on the amino acid side chains of serine, threonine, or tyrosine residues in protein substrates (Manning et al. 2002). By catalyzing the reversible post-translational phosphorylation of Ser/Thr and Tyr residues of substrate proteins, protein kinases serve as signaling integrators that govern most aspects of eukaryotic life. Consequently, there exists a biological imperative to tightly control the catalytic activities of protein kinases, through cyclical phosphorylation of conserved amino acids, protein-protein interactions, and other regulatory post-translational modifications (PTMs). One essential mechanism governing kinase activity is the reversible phosphorylation of conserved amino acid residues within the activation loop, henceforth referred to as the T-Loop (Nolen, Taylor, and Ghosh 2004). In the inactive, unphosphorylated state, the T-Loop adopts a wide range of conformations, including conformations that obstruct substrate binding (Engh and Bossemeyer 2001). Phosphorylation of the activation loop induces an active spatial conformation that is typically more amenable to both binding and enzymatic phosphorylation of protein substrates, and this modification is prevalent across the kinase superfamily (Faezov and Roland L. Dunbrack 2023). Conversely, the removal of phosphate groups in this region by phosphatases (dephosphorylation) usually reverts kinases to an inactive state, generating a reversible switch to turn “on” and “off” kinase-dependent signaling pathways. More recently we hypothesized that ~10% of the Ser/Thr human kinome may also be subject to a conserved form of redox-dependent regulation, including key members of the CAMK, AGC, and AGC-like families of kinases through reversible oxidation of an evolutionarily conserved Cys residue, which lies adjacent to the critical regulatory phosphorylation site on the activation loop (T-loop +2 position) (Byrne et al. 2020).

Understanding the molecular mechanisms underlying kinase regulation by redox-active Cys residues is fundamental as it appears to be widespread in signaling proteins (Xiao et al. 2020; Corcoran and Cotter 2013; Cao et al. 2023) and provides new opportunities

67 to develop specific covalent compounds for the targeted modulation of protein kinases
68 (Weisner et al. 2015). Moreover, redox-active Cys are major sensors of **R**eactive
69 **O**xygen **S**pecies (ROS), such as superoxide and peroxide, which function as
70 endogenous secondary messengers to regulate various cellular processes (Schieber
71 and Chandel 2014; Wani et al. 2011). In particular, the high cell permeability of H_2O_2
72 relative to other ROS species allows it to be sensed intracellularly by reactive Cys,
73 which can differentially impact protein function and cellular localization (Lennicke et al.
74 2015; Rhee et al. 2005). Chemically accessible and reactive Cys residues can transition
75 through several redox states, such as the transient sulfenic acid species (Cys-SOH) and
76 higher order, 'irreversible', sulfinic and sulfonic forms (Cys-SO_2H and Cys-SO_3H)
77 (Forman et al. 2017; Gupta and Carroll 2014). Importantly, in the context of allosteric
78 protein redox regulation, the sulfenic oxidized Cys species can form disulfide linkages
79 with other reactive Cys residues, whilst a sulfenic derivative has also been observed to
80 be stabilized through the formation of a cyclic sulfenamide for tyrosine phosphatase
81 PTP1B (van Montfort et al. 2003; Salmeen et al. 2003). The chemical reactivity, and
82 thus biological susceptibility, of an individual Cys residue to oxidative modification is
83 contingent on the intrinsic pK_a value (where K_a is the acid dissociation constant), which
84 in turn is influenced by networks of interacting amino acids (including phosphorylated
85 amino acids), solvent accessibility, protein-protein interactions, and protein structural
86 dynamics (Poole 2015; Xiao et al. 2020; Soylu and Marino 2016). Unlike
87 phosphorylation, which allosterically communicates with distal sites through positively
88 charged residues that coordinate the phosphate group, it is largely unclear how the
89 redox state of a T-loop localized Cys residue may alter the catalytic activity of a kinase
90 (Garrido Ruiz et al. 2022), although a change in the activation segment conformation is
91 a likely outcome, as demonstrated by careful analysis of Ser/Thr kinases, notably
92 members of the AGC-family kinase AKT (Su et al. 2019).
93 The human AMPK-related kinase (ARK) family, consisting of 14 members (termed
94 BRSK1-2, NUAK1-2, SIK1-3, MARK1-4, MELK, and AMPKα1 and AMPKα2) are
95 fundamental regulators of cellular metabolism, growth, differentiation, and polarity (Shao
96 et al. 2014; Byrne et al. 2020; Shirwany and Zou 2014; Zmijewski et al. 2010), and
97 BRSK1/2 function upstream of redox-based signaling to the pleiotropic transcription

factor Nrf2 (Tamir, Drewry, et al. 2020; Tamir, Bowman, et al. 2020). Like other ARK members, BRSK1/2 possess similar structural organization, consisting of an N-terminal serine/threonine catalytic (kinase) domain, which is followed by a ubiquitin-associated (UBA) domain, a C-terminal spacer, and in some members, a kinase-associated (KA1) domain (Bright, Thornton, and Carling 2009) (Fig 1a). In addition to sharing structural homology, all ARKs (except for MELK) are known to be activated by phosphorylation on their T-Loop by the common upstream regulator LKB1, which is constitutively catalytically active in cells (Lizcano et al. 2004). All of the ARKs contain an activation loop 'T-loop + 2 Cys' residue, which can be prognostic for redox regulation (Byrne et al. 2020), and the catalytic activities of several members have been demonstrated experimentally to be modulated by ROS, including the nominative member, AMPKα, which is both directly and indirectly regulated by redox-state (Auciello et al. 2014; Hinchy et al. 2018; Choi et al. 2001; Shirwany and Zou 2014; Shao et al. 2014). However, the precise mechanisms whereby various ARKs are regulated under redox conditions remain obscure and are likely to be context specific.

The Brain Specific Kinases (BRSKs, also termed Synapses of Amphids Defective [SAD] kinases), consist of two paralogs in vertebrates, termed BRSK1 and BRSK2, and are among the least well-studied of the ARK family (Nie et al. 2012). However, like all other members of the ARK family, BRSKs are downstream signaling targets of the Ser/Thr kinase LKB1 and also have the potential to be regulated 'upstream' by CAMKII, PAK1, and PKA, suggesting signal-dependent phosphorylation as a central regulatory mechanism (Alessi, Sakamoto, and Bayascas 2006; Lizcano et al. 2004; Nie et al. 2012; Bright, Carling, and Thornton 2008). BRSKs are highly expressed in the brain and central nervous system of model organisms, where they exhibit both distinct and redundant molecular functions (Kishi et al. 2005; Nakanishi et al. 2019); furthermore, they are implicated in several human pathologies, in particular neurodevelopmental disorders such as autism spectrum disorder (Saiyin et al. 2017; Li et al. 2020; Deng et al. 2022).

In the current study, we identify a new dominant mechanism for regulation of BRSKs through oxidative modification of conserved Cys residues within the kinase domain. We

demonstrate that the catalytic activities of both BRSK1 and BRSK2 are fine-tuned through oxidative modification of the T-Loop +2 Cys residue, which communicates with a BRSK-specific Cys residue in the APE motif (CPE in BRSKs) within the activation segment. We provide evidence that the T-Loop Cys forms disulfide bonds with the 'CPE' motif Cys and that mutating the CPE-Cys to an alanine increases BRSK activity relative to the wild-type (WT) enzyme. Using a combination of biochemical analysis, structural modeling, and molecular dynamics simulations, we identify regulatory roles for these BRSK-conserved Cys residues and characterize novel intramolecular disulfide-links, providing new insights into BRSK1/2 regulation and the broader AMPK family regulation. Together, these findings highlight complex regulatory processes for BRSK1/2 that are dependent on both phosphorylation and Cys-redox modulation, with broad implications for the other dozen members of the ARK family.

Methods

Recombinant proteins and general reagents

All purchased biochemicals were of the highest purity available, and all recombinant proteins were analyzed by intact mass-spectrometry to confirm the species present. Active, recombinant full-length BRSK1 (2-778) and BRSK2 (2-674) proteins purified from insect Sf21 cells were purchased from MRC PPUU reagents (University of Dundee). Active recombinant LKB1/STRADα/MO25α was purchased from Merck. Gateway pENTR plasmids encoding full length human BRSK1 & BRSK2 were generated as part of the NIH common fund initiative to Illuminate the Druggable Genome (IDG) and was a gift from Dr. Ben Major (Washington University, St. Louis). Antibodies for BRSK1 (#5935), BRSK2 (#5460), DYKDDDDK Tag (D6WB5, #14793), Phospho-AMPKα (Thr172) (#2535), HA-Tag (C29F4, #3724), 6XHiS tag (#2365) and GAPDH (#2118) were from Cell Signaling Technology. Antibodies for Phospho-Tau (rabbit, 44-750G) and GFP (mouse, MA5-15256) were from Invitrogen. The glutathione (ab9443) antibody was obtained from Abcam.

Cloning, Gateway Recombination and Site Directed Mutagenesis

BRSK1 and 2 were cloned into pDest vectors (to express N-terminal Flag or HA tagged proteins) using the Gateway LR Clonase II system (Invitrogen) as per the manufacturer's instructions. pENtR clones were obtained in the form of a Gateway-compatible donor vectors from the laboratory of Ben Major (Washington University in St. Louis). The Gateway LR Clonase II enzyme mixture mediates recombination between the attL sites on the Entry clone and the attR sites on the destination vector. BRSKs were also cloned into a pcDNA3 vector using a standard T4-ligase (NEB) protocol and expressed in frame with a 3C-protease cleavable N-terminal tandem STREP-tag. The catalytic domains of BRSK1$^{29-358}$ or BRSK2$^{14-341}$ were sub-cloned into pET28a (Novagen) to generate N-terminal hexa-His tagged plasmid constructs for expression of BRSK1/2 catalytic domains in *E. coli*. Site-directed mutagenesis was performed using standard PCR-based mutagenic procedures with the Q5 Site-Directed

172 Mutagenesis Kit (New England Biolabs) following the manufacturer's instructions. All
173 plasmids were validated by complete sequencing of the protein coding region.
174
175 **Recombinant BRSK expression and purification**
176 Recombinant human BRSK1$^{29-358}$ or BRSK2$^{14-341}$ proteins, or each of the indicated
177 amino acid substitutions, were produced in BL21 (DE3) pLysS *E. coli* cells (Novagen)
178 and purified in the absence of reducing agents, unless stated otherwise. BRSK1/2
179 expression was induced with 0.5 mM isopropyl-β-D-thiogalactopyranoside (IPTG) for 18
180 h at 18°C and N-terminal His6-tag fusion proteins purified by step-wise affinity
181 chromatography and size exclusion chromatography using a HiLoad 16/600 Superdex
182 200 column (GE Healthcare) equilibrated in 50 mM tris-HCl (pH 7.4), 100 mM NaCl, and
183 10% (v/v) glycerol. Where appropriate for redox assays, recombinant proteins were
184 purified under reducing conditions in the presence of 1 mM DTT, as previously
185 described (Byrne et al. 2020). BRSK proteins expressed from bacteria are
186 unphosphorylated and catalytically inactive, and were activated by incubation with 10 ng
187 of purified LKB1/STRADα/MO25α holoenzyme complex in the presence of 1 mM ATP
188 and 10 mM $MgCl_2$ for 18 h at 4°C. Phosphorylation of BRSK proteins was verified by
189 mass spectrometry and/or Western blotting analysis using a pThr^{172} AMPKα antibody,
190 which demonstrates cross-reactivity for BRSK1/2 T-Loop phosphorylation (Tamir et al.
191 2020).
192
193 **Detection of glutathionylated proteins by immunoblotting**
194 Recombinant BRSK1 and 2 (0.5 µg) were incubated with 50 mM Tris-HCl (pH 7.4) and
195 100 mM NaCl, with 10 mM GSSG or GSH for 30 min at 20°C, and glutathione-protein
196 complexes were detected by immunoblotting after nonreducing SDS-PAGE.
197
198 **BRSK1/2 Kinase assays**
199 BRSK activity assays were performed using microfluidic real-time mobility shift-based
200 assays, as described previously (Byrne et al. 2020; Byrne et al. 2016; Mohanty et al.
201 2016), in the presence of 2 µM of the fluorescent-tagged BRSK1/2 peptide substrate
202 (AMARA; 5-FAM- AMARAASAAALARRR -COOH) and 1 mM ATP. Optimal pressure and

203 voltage settings were established to improve separation of phosphorylated and
204 nonphosphorylated peptides. All assays were performed in 50 mM HEPES (pH 7.4),
205 0.015% (v/v) Brij-35, and 5 mM $MgCl_2$, and the real-time or end point degree of peptide
206 phosphorylation was calculated by differentiating the ratio of the
207 phosphopeptide:peptide. BRSK1/2 activity in the presence of different redox reagents
208 was quantified by monitoring the generation of phosphopeptide during the assay,
209 relative to controls. Data were normalized with respect to control assays, with
210 phosphate incorporation into the peptide generally limited to <20% to prevent depletion
211 of ATP and to ensure assay linearity. Recovery of BRSK activity from oxidative inhibition
212 was assessed by incubating BRSKs with 1 mM hydrogen peroxide, followed by infusion
213 of 2 mM DTT and substrate phosphorylation monitoring in real time. To account for
214 potential variability in LKB1-dependent phosphorylation of BRSK proteins, rates of
215 kinase activity (calculated as pmol phosphate incorporation per min) for each protein
216 was normalized by densitometry to the activation site of phosphorylation signal
217 (established with $pThr^{172}$ AMPKα antibodies and ImageJ software).
218

219 **Differential Scanning Fluorimetry**

220 Thermal shift assays were performed with a StepOnePlus real-time polymerase chain
221 reaction (PCR) machine (Life Technologies) using SYPRO Orange dye (Invitrogen) and
222 thermal ramping (0.3°C in step intervals between 25° and 94°C). All proteins were
223 diluted to a final concentration of 5 μM in 50 mM tris-HCl (pH 7.4) and 100 mM NaCl in
224 the presence or absence of 10 mM DTT and were assayed as described previously
225 (Foulkes et al. 2018). Normalized data were processed using the Boltzmann equation to
226 generate sigmoidal denaturation curves, and average $T_m/\Delta T_m$ values were calculated as
227 previously described (Murphy et al. 2014) using GraphPad Prism software.
228

229 **Human cell culture and treatment**

230 HEK-293T cells were cultured in Dulbecco's modified Eagle medium (Lonza)
231 supplemented with 10% fetal bovine serum (HyClone), penicillin (50 U/ml), and
232 streptomycin (0.25 μg/ml) (Lonza) and maintained at 37°C in 5% CO_2 humidified
233 atmosphere. To examine the effects of oxidative stress on BRSK activity, cells were

234 transiently co-transfected for 24 h with plasmids for expression of full-length, N-terminal
235 tagged (Flag, HA or tandem Strep tag) BRSK1/2 (or Cys-Ala mutants) and EGFP-TAU
236 (Addgene), using 3:1 polyethylenimine (average M_w, ~25,000 Da; Sigma-Aldrich) to total
237 DNA ratio (4 µg BRSK and 2 µg TAU DNA) in a single well of a 24-well culture plate. To
238 investigate inactivation of BRSK by peroxide, cells were incubated for 20 min with 10
239 mM H_2O_2, or buffer control. To establish reversibility of oxidative inhibition, cells were
240 incubated for 20 min with 10 mM H_2O_2, or buffer control followed by a 15 min incubation
241 with 20 mM reduced glutathione (GSH). In all assays, cells were subsequently washed
242 3x in PBS, harvested in bromophenol blue–free SDS sample buffer supplemented with
243 1% Triton X-100, protease inhibitor cocktail tablet, and a phosphatase inhibitor tablet
244 (Roche), or in lysis buffer (50 mM Tris-HCl (pH 7.4), 150 mM NaCl, 1 mM EDTA with 10
245 % (v/v) glycerol and 1 % (v/v) Triton X-100, with 1X protease inhibitor cocktail and 1X
246 HALT phosphatase inhibitor). Lysates were sonicated briefly and clarified by
247 centrifugation at 20 817×*g* for 20 min at 4°C, and supernatants were sampled and
248 diluted 30-fold for calculation of the protein concentration using the Coomassie Plus
249 Staining Reagent (Bradford) Assay Kit (Thermo Fisher Scientific). Cell lysates were
250 normalized for total protein concentration and processed for immunoblotting or immuno-
251 precipitation (IP).
252
253 **Liquid chromatography mass spectrometry (LC-MS) analysis BRSKs**
254 48 h post-transfection, HEK-293T cells overexpressing BRSK1 and 2 (containing an N-
255 terminal 3C cleavable tandem STREP-tag) were treated with 1 mM of the cell
256 permeable chemical oxidant pervanadate for 30 min. Cells were resuspended in ice
257 cold lysis buffer (50 mM Tris-HCl (pH 6.5), 150 mM NaCl, 10 % (v/v) glycerol, 1 % (v/v)
258 NP-40, 100 mM iodoacetamide) and disrupted by passing the cell suspension through a
259 25-gauge needle 10 times. Lysates were clarified by centrifugation at 20 817×g for 20
260 min at 4°C, and recombinant proteins were affinity precipitated using Strep-TACTIN
261 beads and physically eluted using 3C protease for subsequent MS analysis. Affinity
262 precipitated BRSK1/2 and bacterially derived recombinant proteins (10 µg) were diluted
263 (~4-fold and ~18-fold respectively) in 100 mM ammonium bicarbonate (pH 8.0)
264 containing 10 mM iodoacetamide and incubated in the dark for 30 min at room

265 temperature. Samples were subjected to an SP3-based trypsin digestion protocol
266 (adapted from, (Daly et al. 2023)), using 100 mM ammonium bicarbonate (pH 8.0) and
267 0.5 µg of Trypsin gold (Promega). Digested fractions were split 50/50, and one half was
268 treated with dithiothreitol and iodoacetamide as previously described by (Ferries et al.
269 2017). Samples were then subjected to in-house packed strong-cation exchange stage
270 tip clean up, as described by (Daly et al. 2021). Dried peptides were solubilized in 20 µl
271 of 3% (v/v) acetonitrile and 0.1% (v/v) TFA in water, sonicated for 10 min, and
272 centrifuged at 13,000x *g* for 15 min at 4 °C prior to reversed-phase HPLC separation
273 using an Ultimate3000 nano system (Dionex) over a 60-min gradient, as described by
274 (Ferries et al., 2017). For affinity precipitated BRSK preparations from human cells, all
275 data acquisition was performed using a Thermo QExactive mass spectrometer (Thermo
276 Scientific), with higher-energy C-trap dissociation (HCD) fragmentation set at 30%
277 normalized collision energy for 2+ to 4+ charge states. MS1 spectra were acquired in
278 the Orbitrap (70K resolution at 200 *m/z*) over a range of 300 to 2000 *m/z*, AGC target =
279 1e6, maximum injection time = 250 ms, with an intensity threshold for fragmentation of
280 1e3. MS2 spectra were acquired in the Orbitrap (17,500 resolution at 200 *m/z*),
281 maximum injection time = 50 ms, AGC target = 1e5 with a 20 s dynamic exclusion
282 window applied with a 10 ppm tolerance. For bacterially derived recombinant proteins,
283 all data acquisition was performed using a Thermo Fusion Tribrid mass spectrometer
284 (Thermo Scientific), with higher-energy C-trap dissociation (HCD) fragmentation set at
285 32% normalized collision energy for 2+ to 5+ charge states. MS1 spectra were acquired
286 in the Orbitrap (120K resolution at 200 *m/z*) over a range of 400 to 2000 *m/z*, AGC
287 target = 100%, maximum injection time = auto, with an intensity threshold for
288 fragmentation of 2.5e4. MS2 spectra were acquired in the Orbitrap (30k resolution at
289 200 *m/z*), maximum injection time = dynamic, AGC target = auto with a 20 s dynamic
290 exclusion window applied with a 10 ppm tolerance. For disulfide analysis (regardless of
291 sample type), raw data files were converted into mgf format using MSConvert, with peak
292 picking filter set to “2- ” and searched with the MASCOT search engine (Perkins et al.
293 1999); searching the UniProt Human Reviewed database (updated weekly, accessed
294 January 2023) (UniProt 2023) with variable modifications = carbamidomethylation (C),
295 oxidation (M), phosphorylation (ST), instrument type = electrospray ionization–Fourier-

transform ion cyclotron resonance (ESI-FTICR) with internal fragments from 200-2000 *m/z*, MS1 mass tolerance = 10 ppm, MS2 mass tolerance = 0.01 Da. The crosslinking option was selected for the accessions Q8TDC3 or Q8IWQ3 with strategy set to Brute-force, for InterLink, IntraLink and LoopLink for the linker “Xlink: Disulfide (C)”. For the best MASCOT scoring peptide spectrum match (PSM) for a disulfide-containing peptide, the mgf file was extracted from the raw file and imported into a custom R script for re-drawing and manual annotation. Immunoprecipitated samples were additionally analyzed using PEAKS Studio (version XPro) using the same database, mass tolerances and modifications as previously described. PEAKS specific search settings: instrument = Orbi-Orbi, Fragmentation = HCD, acquisition = DDA, De Novo details = standard and a maximum of 5 variable PTMs possible. PEAKS PTM mode was enabled and filtering parameters of De Novo score >15, -log10P(value) >30.0, Ascore >30.0.

Phylogenetic Analysis

We identified and aligned diverse BRSK-related sequences from the UniProt reference proteomes database (downloaded on June 7, 2022) (UniProt 2023) using MAPGAPS (Neuwald 2009). From these hits, we manually curated a diverse set of sequences, then inferred a maximum-likelihood phylogenetic tree with IQ-TREE version 2.0.7 (Minh et al. 2020). Branch support values were generated using ultrafast bootstrap (Hoang et al. 2018) with 1000 resamples. The optimal substitution model was LG+R6 based on the Bayesian Information Criterion as determined by ModelFinder (Kalyaanamoorthy et al. 2017). The consensus tree was used as our final topology. Subsequent analyses were performed using the ETE3 Toolkit (Huerta-Cepas, Serra, and Bork 2016).

Molecular Dynamics Simulations

The starting model for molecular dynamics (MD) simulations was selected to provide an accurate representation of the protein kinase in its active-like conformation. To achieve this, we utilized an AlphaFold model of the BRSK2 kinase domain, corresponding to residues 14-267, in an active-like conformation. The average pLDDT score for the portion of the AlphaFold model employed in MD simulations was calculated to be 89.18%, indicating high confidence and accuracy (Jumper et al. 2021). Starting

327 structures were prepared using the CHARMM-GUI interface which allowed for
328 incorporation and parameterization of T-Loop phosphorylation, cysteine to alanine
329 mutation, and oxidative cysteine modification (Brooks et al. 2009; Lee et al. 2016; Jo et
330 al. 2014). Cysteine 176 (T+2) and 183 (CPE motif) were each mutated to alanine,
331 sulfenic acid, or sulfonic acid forms. The protein was solvated in a cubic box of TIP3P
332 water molecules, and counterions were added to maintain neutrality. The final systems
333 contained ~ 54,000 atoms.
334 Prior to production runs, the system was subjected to minimization and equilibration
335 protocols, using previously described parameters (Yeung et al. 2021; Venkat et al.
336 2023). Initially, a steepest descent energy minimization was performed to relax the
337 system, followed by equilibration at constant volume and temperature (NVT) and
338 constant pressure and temperature (NPT). Each equilibration stage was carried out for
339 125 ps with 1 fs time steps. Following equilibration, long-range electrostatics were
340 calculated via particle mesh Ewald (PME) algorithms using the GROMACS MD engine
341 (Van Der Spoel et al. 2005). Three 100 ns production molecular dynamics (MD)
342 replicates were conducted at a 2fs time-step using the CHARMM36 forcefield for each
343 starting model (Brooks et al. 2009). The resultant MDs were visualized with PyMOL
344 (Schrodinger 2015) and analyzed in the python environment (Michaud-Agrawal et al.
345 2011).
346
347 **SDS-PAGE and Western blotting**
348 Processed cell lysates and purified recombinant proteins were loaded onto 10% (v/v)
349 SDS-PAGE gels, separated by electrophoresis and transferred onto nitrocellulose
350 membranes using a semi-dry transfer system at 300 mA for 45 minutes. Nitrocellulose
351 membranes were blocked with 4% (w/v) Bovine Serum Albumin (BSA, Rockland) in
352 Tris-buffered saline with 0.1% (v/v) Tween-20 (TBST) for 1 h at room temperature and
353 incubated overnight at 4°C with the indicated primary antibodies. Protein was detected
354 using specific secondary IRdye conjugated antibodies (Donkey anti Rabbit IRdye800cw
355 or Goat anti Mouse IRdye680) and imaged using LI-COR Odyssey imaging system, or
356 HRP-conjugated secondary antibodies and enhanced chemiluminescence reagent
357 (Pierce ECL Plus, Thermo Fisher Scientific). All antibodies were prepared in a solution

358 of BSA dissolved in TBST and diluted according to manufacturer's instructions.
359 Reducing and non-reducing SDS-page for BRSK proteins was performed as previously
360 described (Byrne et al, 2020).

361 Two-color Western blot detection method employing infrared fluorescence was used to
362 measure the ratio of Tau phospho serine 262 to total Tau. Total EGFP Tau was detected
363 using a mouse anti GFP antibody and visualized at 680 nm using goat anti mouse
364 IRdye 680 while phospho-tau was detected using a Tau phospho serine 262 specific
365 antibody and visualized at 800 nm using goat anti rabbit IRdye 800. Imaging was
366 performed using a LI-COR Odyssey Clx with scan control settings set to 169 µm,
367 medium quality, and 0.0 mm distance. Quantification was performed using Li-COR
368 image studio on the raw image files. Total Tau to phospho Tau ratio was determined by
369 measuring the ratio of the fluorescence intensities at 800 nm (pTau) to those at 680 nm
370 (total tau) for each band. Statistical analysis was conducted in GraphPad Prism, to
371 determine significant differences between experimental groups. Data is presented as
372 mean ± standard error of the mean (SEM).

373

374 **Size Exclusion Chromatography with multi-angle Light scattering (SEC-MALS)**

375 The oligomeric state of recombinant BRSKs was characterized by in-line Size Exclusion
376 Chromatography-Multi-Angle Laser Light Scattering (SEC-MALS). Purified BRSK
377 proteins (1 mg mL^{-1}) were applied directly to a HiLoad 16/60 Superdex 200 attached to
378 an ÄKTA pure fast protein liquid chromatography (FPLC) system equilibrated in 10 mM
379 Tris-HCl pH 7.4, 150 mM NaCl at a flow rate of 0.7 mL min^{-1}. Eluted protein was
380 detected by a MALLS detector and a differential refractive index (DRI) detector (DAWN
381 HELEOS-II and Optilab TrEX; Wyatt Technology, Santa Barbara, CA, USA). Data was
382 analyzed using ASTRA v6.1 software (WYATT). The system was calibrated using BSA
383 prior to data collection with BRSK1/2 proteins.

384

Results

Full-length BRSKs exhibit Redox-Sensitivity

Full length BRSK kinases share similar domain architecture to other ARK family members, including a ubiquitin associate domain (UBA) and kinase associated domain (KA1) following their kinase domain (Fig 1a). Due to the absence of known endogenous substrates selectively phosphorylated by BRSK1 or 2 (Tamir et al. 2020), we utilized a EGFP-Tau overexpression system in HEK-293T cells to assess BRSK activity (Yoshida and Goedert 2012). BRSK1 and 2, when co-expressed with EGFP-Tau, induced substantial phosphorylation of Tau at Ser 262, a modification lost in kinase-dead (KD) mutants with the catalytic aspartate in the 'HRD' motif mutated to alanine ($D146^{BRSK1}$ or $D141^{BRSK2}$), as shown in Figure 1b. The catalytic output of purified full length human BRSK1 & 2 purified from Sf21 cells was next monitored in real-time using a microfluidic kinase assays system and a generic ARK family substrate peptide AMARA (5-FAM-AMARAASAAALARRR -COOH), which is phosphorylated by BRSK1/2, but not the upstream kinase LKB1. In the absence of reducing agents (buffer alone), detectable peptide phosphorylation was extremely low for both kinases and ablated in the presence of H_2O_2 (Fig 1c). In contrast, inclusion of DTT enhanced BRSK1 & 2 activity by several orders of magnitude (Fig 1c). Moreover, H_2O_2-dependent inhibition of catalysis could be reversed, and even increased relative to basal activity, with the subsequent addition of a bolus of the reducing agent DTT (Fig 1c). BRSK proteins were rapidly activated by DTT in a concentration-dependent manner, suggesting an obligate requirement of an appropriate reducing environment in order to enable catalytic activity (Fig 1d and Supp Fig 2a-b). Similarly, basal BRSK activity was inhibited by a gradient of H_2O_2 (Fig 1e, Supp Fig 2c-d). Western blotting revealed a dose-dependent and statistically significant decrease in BRSK-mediated pTau signal following incubation of HEK-293T cells with 10 mM peroxide for 10 minutes, with little alteration in total transfected Tau protein (Fig 1f). At the highest concentrations of peroxide treatment, we detected a reduction in total BRSK protein levels, suggesting a potential loss of stability for both kinases. Chronic oxidative stress was next stimulated by supplementing culture medium with (2 U/mL) glucose oxidase to facilitate constitutive steady-state generation

415 of H_2O_2 (Askoxylakis et al. 2011, Mueller et al. 2009, Truong et all, 2016). This revealed
416 a time dependent depletion of BRSK1 and 2 associated Tau phosphorylation (Supp Fig
417 2e-f). Importantly, H_2O_2-dependent loss of pTau could be reversed following exposure of
418 the cells to the physiological antioxidant glutathione (GSH) (Fig 1g). These findings
419 suggest that reversible oxidative modulation is relevant to BRSK1/2 kinase-dependent
420 signaling in human cells, which can be recapitulated *in vitro*.
421

422 **Mass spectrometric evidence that BRSK cysteine pairs can form intramolecular**
423 **disulfide bonds**
424

425 To identify residues that may contribute to redox regulation of BRSKs, we analyzed
426 tryptic peptides derived from precipitated full-length cellular BRSK1 and BRSK2 by
427 liquid chromatography–tandem mass spectrometry (LC-MS/MS). HEK-293T cells
428 transiently over-expressing Strep-tagged BRSK proteins were lysed in the presence of
429 the alkylating agent iodoacetamide to covalently block free thiol groups. LC-MS/MS
430 revealed the presence of intramolecular bonds between $C147^{BRSK1}$ **-** $C153^{BRSK1}$ and
431 $C191^{BRSK1}$ **-** $C198^{BRSK1}$ and $C132^{BRSK2}$ **-** $C138^{BRSK2}$ and $C176^{BRSK2}$ **-** $C183^{BRSK2}$ (Fig 2a).
432 Of note, all identified disulfide forming Cys residues were located in the kinase domains
433 of the two proteins, in close proximity to known catalytic or regulatory motifs. $C147^{BRSK1}$
434 **-** $C153^{BRSK1}$ and $C132^{BRSK2}$ **-** $C138^{BRSK2}$ structurally link the HRD motif in the catalytic
435 loop to the preceding E-helix, and $C191^{BRSK1}$ **-** $C198^{BRSK1}$ and $C176^{BRSK2}$ **-** $C183^{BRSK2}$
436 couple the T-loop Cys to the Cys residue of the CPE motif in BRSK1/2 (equivalent to the
437 APE motif in most kinase activation segments) (Fig 2b). To study these reactive Cys
438 residues in the context of catalysis, we purified the unphosphorylated catalytic domain
439 of human $BRSK1^{29-358}$ (BRSK1cat) or $BRSK2^{14-341}$ (BRSK2cat) to homogeneity from *E.*
440 *coli*. As expected, both truncated variants of BRSK were completely inactivate in our
441 AMARA-based kinase assay, but could be 'switched on' following incubation with the
442 physiological upstream regulator LKB1 (Fig 2c). Of note, despite sharing ~95%
443 sequence identity within their kinase domain, LKB1-activated BRSK2 had higher
444 catalytic activity compared to BRSK1 (Fig 2c). Moreover, and in support of our previous
445 findings for full-length BRSK proteins (Fig1), incubation of LKB1-activated WT BRSK1
446 or 2 with DTT greatly increased activity (Fig 2c). These data are consistent with

447 regulatory Cys-based modification of the kinase domain under oxidative conditions,
448 which can be reversed with a reducing agent *in vitro*.
449
450 **Emergence and structural location of cysteines residues in BRSK proteins**
451 Reversible redox regulation of signaling proteins typically requires sulfenyl derivatization
452 of an exposed Cys residue(s) (Heppner, Janssen-Heininger, and van der Vliet 2017).
453 Cys is the second least abundant amino acid in the vertebrate proteome, and conserved
454 surface exposed Cys side chains can function as redox "hotspots" (Fomenko, Marino,
455 and Gladyshev 2008; Su et al. 2019; Xiao et al. 2020). Previously, we established that
456 all 14 members of the ARK family kinases, including BRSK1 and 2, contain a T-loop + 2
457 Cys residue. This residue is equivalent to the redox sensitive C199 found in PKA
458 (Humphries, Juliano, and Taylor 2002) and is prognostic of redox regulation for multiple
459 human Ser/Thr kinases (Byrne et al., 2020). Of the ARK family kinases that we
460 previously analyzed, AMPKα1, SIK1-3 and MELK were all acutely inhibited by H_2O_2 in a
461 reversible manner *in vitro*, which we attributed to sulfenylation of the activation segment
462 Cys, based on biochemical and evolutionary analysis (Byrne et al., 2020). The T-loop +
463 2 Cys corresponds to $C191^{BRSK1}$ and $C176^{BRSK2}$ in BRSK1 and 2 respectively. This
464 residue is located within the canonical activation segment, in close proximity to the
465 regulatory site of LKB1 phosphorylation. Interestingly, mapping of Cys residues across
466 the human ARK family reveals several conserved Cys located throughout their kinase
467 domains (Fig 3a and b). However, these studies also reveal a distinguishing Cys
468 residue that is unique to the catalytic domain of human BRSKs, which is located at the
469 canonical alanine position of the "APE" motif, converting it to "CPE" ($C198^{BRSK1}$/
470 $C183^{BRSK2}$ (Fig 3b). Of note, the unusual CPE Cys forms an intramolecular disulfide with
471 the T-loop +2 Cys (Fig 2a). Intramolecular dimers incorporating T-loop Cys have also
472 been identified in MELK and AKT2 (Cao et al. 2013; Huang et al. 2003). MELK is
473 exceptional in that it possesses both a T-loop +1 as well as a T-loop +2 Cys, where the
474 T-loop +1 Cys forms an intramolecular disulfide with a Cys proximal to the DFG motif
475 and the T-loop +2 can form an intermolecular disulfide potentiating dimerization (Cao et
476 al. 2013). In the case of AKT2, the T-loop +2 Cys forms an intramolecular disulfide with
477 a Cys equivalent to that seen in MELK (Huang et al. 2003). In addition to the T+2 Cys,

478 most human ARK family members (with the exception of MELK) contain an additional
479 conserved Cys positioned 7 residues upstream of the HRD motif (HRD -7 Cys) located
480 in the E-helix (Fig 3a and b). BRSKs share the HRD -7 Cys ($C147^{BRSK1}$/ $C132^{BRSK2}$), but
481 further diverge from other ARK family members with the insertion of an additional
482 potential disulfide bond-forming Cys residues preceding the HRD motif in the catalytic
483 loop (CHRD-Cys, $C153^{BRSK1}$/ $C138^{BRSK2}$ in Fig 3a and b).
484
485
486 **Phylogenetic analysis of BRSK protein sequences**
487 A sequence-based analysis reveals the emergence of an early BRSK1 variant, which
488 we term 'proto-BRSK1' that distinguishes it from the closely related AMPKs (Supp Fig
489 1a). This is followed by a subsequent expansion of BRSK1 and 2 sequences that
490 coincides with the appearance of vertebrates (Fig 3c). Sequence alignment of BRSK
491 catalytic domains from a diverse array of organisms, including the ancestral paralog and
492 invertebrate specific proto-BRSK1, confirmed general sequence similarity and tight
493 conservation of T-loop and HRD proximal Cys 'pairs' (Fig 3d). Interestingly, all BRSK
494 domains also possess a Cys residue in the N-terminal β2-β3 loop ($C54^{BRSK1}$/ $C42^{BRSK2}$),
495 and BRSK2 contains an additional residue at this site, $C39^{BRSK2}$ (Fig 3d). The
496 diversification of BRSKs from AMPKs also correlates with an increase in the total
497 number of Cys residues in the kinase domain (Supp Fig 1a). Analysis of 2805 ARK-
498 related sequences confirmed significant conservation of the T-loop + 2 and HRD -7 Cys,
499 which were found respectively in ~18 % and ~10 % of ePKs across diverse eukaryotic
500 species (Fig 3e). These Cys residues were invariant in vertebrate BRSK sequences, as
501 were the BRSK specific CPE and HRD -1 Cys residues (Fig 3e). Unsurprisingly,
502 substitution of the APE Ala (PKA position 206, found in ~65 % of ePKs) with a Cys is
503 extremely uncommon (~1 %) in nearly all protein kinases, given the critical role of this
504 motif in stabilizing the C-lobe and substrate interactions (Supp Fig 1b). The distribution
505 of amino acids at HRD -1 position is much more variable in ePKs, with Ile and Val being
506 most commonly conserved (~36 and 30 % respectively) and a Cys appearing with
507 similar low frequency (~ 2% (Supp Fig 1b). The high degree of conservation observed
508 for these Cys residues within vertebrate BRSKs indicates that they play critical

509 functional or structural roles in these kinases (Fig 3e). This further suggests that
510 diversification of the BRSKs in metazoans correlated with the accumulation of close
511 proximity Cys 'pairs' with the potential to form regulatory disulfide bonds.
512
513 **Cysteine residues within the kinase domain fine-tune BRSK activity**
514 To assess the role of BRSK domain Cys residues in modulating catalytic activity, we
515 expressed and purified wild-type (WT) and Cys-to-Ala variants of the BRSK1 and 2
516 kinase domains in *E. coli*. These Cys-to-Ala variants included T-loop +2 Cys mutants
517 (C191A^{BRSK1} and C176A^{BRSK2}), and T-loop CPE mutants (C198A^{BRSK1} and C183A^{BRSK2}),
518 expressed either in a WT or mutant T-loop +2 Cys background (C191/198A^{BRSK1} and
519 C176/183A^{BRSK2}). We also generated double mutants of the Cys residues upstream of
520 the HRD motif (C147/153A^{BRSK1} and BRSK2 C132/138A^{BRSK2}), and the unique N-
521 terminal Cys pair in BRSK2 (C39/42A^{BRSK2}). All recombinant BRSK proteins were
522 expressed in *E. coli* and purified without DTT. Crucially, we were able to detect
523 intramolecular disulfide bonds (C191^{BRSK1} - C198^{BRSK1} and C176^{BRSK2} - C183^{BRSK2}) in
524 the WT proteins by LC-MS/MS (Supp Fig 3). Interestingly, we could only identify an
525 HRD proximal disulfide bond (C147^{BRSK1} - C153^{BRSK1}) in BRSK1 under these specific
526 experimental conditions (Supp Fig 3). We next probed for mixed disulfide formation in
527 the presence of glutathione, using an antibody that recognizes glutathionylated proteins.
528 We detected robust glutathionylation of both BRSK1 and BRSK2 in the presence of
529 either reduced (GSH) or oxidized (GSSG) glutathione, and the signal strength inversely
530 correlated with the presence of DTT (Supp Fig 4a). Of note, all of the BRSK Cys-to-Ala
531 mutants studied here could be readily glutathionylated, which supports the existence of
532 multiple reactive Cys residues within the kinase domains of BRSK1 and 2. To detect
533 alterations in redox regulation, all BRSK proteins were first activated by incubation with
534 LKB1, and T-loop phosphorylation was confirmed by immunoblotting (Supp Fig 4b). The
535 active BRSK1/2 kinases were then assayed using the specific AMARA peptide in the
536 presence or absence of fixed concentrations of DTT, and kinase activity was normalized
537 to pBRSK signal derived from Supp Fig 4b. In agreement with our previous findings with
538 full-length BRSKs, DTT was strongly activating for WT variants of both kinases, and this
539 effect was severely blunted for the T-loop +2 Cys-Ala mutants, which exhibited lower

basal rates of peptide phosphorylation. This is entirely consistent with our previous observations for Cys-based mutants of analogous residues in a range of distinct Ser/Thr kinases (Byrne et al. 2020) (Fig 4a and b). Of note, despite sharing ~95% sequence identity within their kinase domain, LKB1-activated BRSK2 demonstrated enhanced catalytic activity compared to BRSK1 (Fig 4b compared to a). Perhaps unsurprisingly, given their distant location on an N-lobe loop, mutation of the BRSK2 exclusive $C39^{BRSK2}$ and $C42^{BRSK2}$ residues had limited effect on the activity of BRSK2 (Fig 4b). In contrast, tandem mutation of the HRD proximal Cys residues resulted in pronounced abrogation of kinase activity, regardless of assay conditions for both kinases (Fig 4a and b). Given the near absolute conservation of the HRD -7 Cys in the ARK family of protein kinases, it is possible that this residue ($C147^{BRSK1}$ and $C132^{BRSK2}$) is functionally important for catalytic activity in some yet unidentified capacity. Interestingly, mutation of the CPE motif Cys (T-loop +9 Cys), and *de facto* restoration of the canonical APE motif, were insufficient to blunt DTT-dependent activation of either kinase. Moreover, this mutation, which would eliminate $C191^{BRSK1}$ - $C198^{BRSK1}$ and $C176^{BRSK2}$ - $C183^{BRSK2}$ disulfide bonds, increased basal (non-DTT stimulated) catalytic activity by 1.5-2-fold for both kinases. WT forms of BRSK2, and in particular BRSK1, were strongly inhibited by oxidative conditions, even when assays were preceded by DTT-dependent activation (Fig 4c and d). Unsurprisingly, the low levels of detectable $C191A^{BRSK1}$ and $C176A^{BRSK2}$ activity that could be measured following stimulation by DTT were completely abolished following the addition of H_2O_2. In contrast, CPE mutants ($C198A^{BRSK1}$ and $C183A^{BRSK2}$) were sharply activated by DTT but still exhibited further oxidative inhibition (Fig 4c and d), although to a lesser extent than their WT counterparts, particularly in the case of BRSK1.

To ensure that the observed variations in activity between variants of BRSK1/2 were not a consequence of structural impairment, we also performed differential scanning fluorometry (DSF) to assess protein folding and stability. Incubation of WT BRSK1 and 2 with DTT had no measurable effect on the thermal stability of either protein, suggesting that chemical disruption of pre-formed disulfide bonds had a minimal detectable impact on global protein stability, despite greatly increasing kinase activity (Supp Fig 4c). These assays also revealed only minor perturbations in protein thermal stability due to the

571 incorporation of specified Cys-to-Ala mutants. Interestingly, we observed a consistent
572 decrease in T_m values for C147/153A^{BRSK1} and C132/138A^{BRSK2} (ΔT_m ~ -2 °C),
573 suggesting a modest decrease in protein stability, and increased T_m values for CPE
574 mutants (C198A^{BRSK1} and C183A^{BRSK2}; ΔT_m ~ +3 °C) (Supp Fig 4d).
575
576 **Cellular analysis of BRSK Cys-based regulation**
577 We next evaluated the relative contributions of the conserved T-loop Cys residues to
578 BRSK redox sensitivity in a cellular context using our EGFP-Tau HEK-293T co-
579 expression system and full length BRSK proteins. Mirroring our peptide-based kinase
580 assays, loss of the T-loop +2 Cys residue evoked a marked decrease in BRSK-
581 dependent Tau phosphorylation **(**Fig 5a and 5b)**.** In contrast, mutation of the CPE Cys to
582 an alanine consistently increased overall Tau phosphorylation (~1.5 and ~1.2 fold
583 increase relative to WT BRSK1 and BRSK2 respectively) (Fig 5). Interestingly, the CPE
584 mutations preserved BRSK redox sensitivity in cells treated with hydrogen peroxide,
585 and inclusion of GSH was sufficient to restore BRSK-dependent pTau signals. Finally,
586 we extended our analysis to consider the BRSK1 and 2 HRD motif proximal cysteines,
587 and the BRSK2 exclusive C39/C42 pair. As predicted, Tau phosphorylation by BRSK2
588 C39/42A (which closely matched the activity profile of WT BRSK2 in our *in vitro* kinase
589 assays (Fig 4)) was comparable to that observed for WT (but still less than hyper-active
590 BRSK2 C183A) and was also similarly inhibited by the presence of H_2O_2 (Supp Fig 4e).
591 Using the AMARA peptide as a substrate, we previously demonstrated that BRSK1
592 C147/153A and BRSK2 C132/138A were catalytically compromised (in a manner
593 resembling the respective T-loop + 2 Cys-Ala mutants (Fig 4)). It is consistent that
594 BRSK2 C132/138A was unable to increase pTau signal above background levels (Supp
595 Fig 4e). Finally, we were unable to detect BRSK1 C147/153A protein expression in
596 transfected cell lysates, which may indicate a loss of stability for this protein (Supp Fig
597 4e).
598
599 **Cysteine modifications alter critical structural interactions required for kinase**
600 **allosteric regulation**
601

602 We next sought to investigate the structural basis for redox-dependent regulation of
603 BRSK activity using molecular modeling and molecular dynamics (MD) simulations. Our
604 *in vitro* analysis established that oxidative conditions inhibit the active, T-loop
605 phosphorylated form of BRSKs, and so our simulations were performed on an 'active'
606 conformation of BRSK2 generated using AlphaFold2 (see methods). Cysteine residues
607 can undergo both reversible (sulfenic) and irreversible (sulfonic) oxidation, and so
608 sulfenic acid or sulfonic acid forms of Cys were incorporated at the C176^{BRSK2} and
609 C183^{BRSK2} positions. Additionally, the impact of a non-redox active 'silent' Ala residue
610 was also modelled at these sites.
611 The T+2 C176^{BRSK2} is in close proximity to threonine T174^{BRSK2}, phosphorylation of
612 which stabilizes the kinase domain in an active conformation through salt bridge
613 interactions with charged residues in the catalytic loop (Fig 6a). In particular, R140^{BRSK2}
614 in the canonical HRD motif coordinates with the phosphate group of pT174^{BRSK2} (Nolen,
615 Taylor, and Ghosh 2004). Simulations demonstrate that the R140^{BRSK2}-pT174^{BRSK2} salt
616 bridge is preserved across the entire MD simulation, as demonstrated by the contact
617 map (Fig 6b). In the C176Ala^{BRSK2} simulations, the coordination between R140^{BRSK2} and
618 pT174^{BRSK2} is partially attenuated due to an increase in the flexibility of pT174^{BRSK2} (Fig
619 6c). This predicted increase in flexibility may explain the loss of BRSK2 catalytic activity
620 for C176A^{BRSK2} mutant (Fig 4). However, oxidative modification of C176^{BRSK2} did not
621 result in a substantial disruption of the salt bridge interaction (Fig 6d,e). As such, it is
622 unclear at this stage precisely how oxidation of the T+2 Cys exerts is regulatory effect
623 on BRSK2 kinase activity.
624 In contrast to C176^{BRSK2}, C183^{BRSK2} within the CPE motif is buried in the C-terminal lobe
625 of the kinase domain, and the SH group of C183^{BRSK2} is pointed toward a canonical salt
626 bridge that forms between the glutamate (E185^{BRSK2}) in the APE/CPE motif and
627 R259^{BRSK2} in the I-helix (Fig 6f). The E185-R259 salt bridge is a eukaryotic protein
628 kinase (EPK)-specific interaction that is critical for maintaining the EPK fold and for
629 allosterically coupling the T-Loop to distal substrate binding and regulatory sites (Yang
630 et al. 2012; Oruganty and Kannan 2012). The selective conservation of Cys in place of
631 Ala in the APE motif represents an interesting divergence of BRSKs from other ARK
632 family kinases (Fig 3e, Supp fig 1). When C183^{BRSK2} is in a reduced form or mutated to

633 an alanine, the E185-R259 is maintained throughout the MD simulation (Fig 6g/i)
634 Remarkably, in simulations incorporating oxidative modification of C183^{BRSK2} we
635 observed the immediate breaking of the E185-R259 salt bridge, and this contact
636 remains broken throughout the simulation (Fig 6h,j). Oxidation of C183^{BRSK2} to either
637 sulfenic or sulfonic acid rewires this salt bridge, with R259^{BRSK2} exclusively interacting
638 with the oxidized C183^{BRSK2} while E185^{BRSK2} pivots outward and becomes more solvent-
639 exposed. Thus, oxidized C183^{BRSK2} mediated disruption of E185-R259 ^{BRSK2} salt bridge
640 represents a unique inactive state in BRSKs which breaks the allosteric network that
641 allows cross-communication between the T-loop and the C-Lobe.
642 Surprisingly, simulations incorporating intramolecular disulfide bonds identified in
643 MS/MS experiments did not indicate any major changes in dynamics resulting from
644 either the Cys132-138 or the Cys176-183 disulfide bond formation. Most of the
645 fluctuations in these simulations were confined to the G-Loop and β3-αC loop, which
646 are distal from the disulfide bonds (Supp. Fig 5)
647
648 **Recombinant BRSK proteins form limited protein dimers**
649 Several ARK family members form disulfide bond-dependent dimers (Nayak et al. 2006;
650 Marx et al. 2010; Cao et al. 2013). To evaluate the formation of intermolecular
651 disulfides, we subjected purified kinase domains of BRSK1 and 2 isolated from *E. coli* to
652 non-reducing SDS-PAGE, followed by western blotting to probe for higher order BRSK
653 structures (Fig 7). This revealed multiple species of each kinases possessing drastically
654 decreased electrophoretic mobility compared to the major BRSK1/2 monomer bands.
655 These species increased in abundance in the presence of H_2O_2 and were absent when
656 DTT was included. Of particular significance was the appearance of a prominent
657 oxidation-dependent species at ~70 kDa, the approximate molecular weight of a BRSK
658 dimer. Consistently, all higher molecular weight species resolved into a single monomer
659 band after reducing (+DTT) SDS-PAGE, which strongly implicates disulfide bond-
660 dependent oligomerization. Curiously, mutation of the T+2 Cys had no discernable
661 effect on the formation of BRSK oligomers, although this is consistent with our previous
662 observation of multiple reactive Cys residues in BRSKs that may be capable of forming
663 a broad variety of intermolecular disulfide bonds. However, it is noteworthy that even in

664 the presence of peroxide, the majority of the BRSK1 and 2 proteins existed as a
665 monomeric species, which suggests that oligomerization is unlikely to be the primary
666 driver of oxidative inhibition that we detect in kinase-based peptide assays.
667 Furthermore, we detected interactions between BRSK1 and BRSK2 (suggesting homo-
668 and heterodimer formation) after co-immunoprecipitation of alternatively tagged variants
669 of the full length proteins overexpressed in the HEK-293T system (Supp Fig 6a).

670 Using SEC-MALS, we confirmed that BRSK1 and 2 (purified in the absence of DTT)
671 were near-uniformly monomeric in solution, but possessed the potential to self-
672 associate and form dimers. The molar mass points across the monomer peak indicates
673 a high degree of homogeneity (weight-average molar mass M_w = ~42 kDa ± 0.99 % and
674 ~43 kDa ± 0.25 %, respectively Supp Fig 6b and c). Interestingly, the BRSK2 spectra
675 included a high molecular weight shoulder of an approximate dimer size (M_w = ~75 kDa
676 ± 2.1 %) that exhibited non-uniform molar mass points indicative of a heterogenous
677 population (likely as a consequence of poor separation between the two peaks and
678 higher order oligomers). SEC-MALS also confirmed the presence of a BRSK species of
679 approximate dimer size (M_w = ~80 kDa) for $C183^{BRSK2}$ that was noticeably absent for
680 $C176^{BRSK2}$ (Supp Fig 6d and e). Although the major species observed for both mutants
681 was a monomer, the inability to detect dimer-like peaks for $C176^{BRSK2}$ may suggest that
682 the T-+2 Cys plays a role in dimerisation. Although we have searched for BRSK1/2
683 inter-molecular disulfide bonds in our LC-MS/MS data in an attempt to characterize the
684 mechanism of dimer formation, we were unable to identify any inter-molecular linked
685 peptides. This is likely due to the extremely low abundance of these dimeric species in
686 this sample (thus yielding a very small proportion of inter-linked tryptic peptides) and/or
687 because inter-molecular disulfide linked tryptic peptides are too large for identification
688 using this analytical pipeline. Collectively these findings confirm that the isolated kinase
689 domains of both BRSKs primarily occupy a largely monomeric conformation and can
690 form limited higher order redox-sensitive oligomers via covalent S-S bonds *in vitro*.
691 However, although reversible oxidation-based inactivation of BRSK1 and 2 is apparent
692 in full-length BRSK1 and 2, it remains to be determined to what extent multimerization
693 modulates BRSK catalytic activity (Fig 8) or how these mechanisms might contribute to
694 signaling-based interactions in cells.

695

696 **Discussion**

697 Redox regulation of kinases and other signaling molecules is a rapidly expanding field
698 of research, which has recently extended far beyond the early observations of oxidative
699 inhibition in protein tyrosine phosphatases (Brandes, Schmitt, and Jakob 2009). More
700 recent enquiries have provided strong evidence for direct regulative oxidative
701 modification of Met and Cys residues across divergent protein kinase families, providing
702 temporal and spatial control of their catalytic outputs (Corcoran and Cotter 2013; Truong
703 and Carroll 2013; Jarvis, Hughes, and Ledgerwood 2012). However, despite the
704 prevalence of this regulatory mechanism, the structural basis to explain how redox-
705 active cysteines contribute to allosteric control of catalytic activity is still in its infancy. In
706 this study, we demonstrate, for the first time, that two T-loop +2 Cys-containing
707 members of the ARK family, BRSK1 and 2, are reversibly inactivated by oxidative-
708 dependent mechanisms *in vitro* and in human cells. Moreover, we uncover a
709 multifaceted redox-activity profile for human BRSKs, involving functional Cys-pairs that
710 are conserved within the catalytic domains of these understudied enzymes. In contrast
711 to Ser/Thr kinases such as Aurora A, where a single Cys residue is the dominant driver
712 of redox-sensitivity (Byrne et al. 2020; Tsuchiya et al. 2020), BRSK1 and 2 possess
713 multiple sulfenylation-prone Cys residues. Additionally, the close proximity of distinct
714 Cys 'pairs' permits the formation of two intramolecular disulfide bonds: the first forming
715 between two HRD-motif proximal sites, and the second bridging the conserved T-loop +
716 2 and unique 'CPE' motif Cys residues. We propose a model where disulfide bond
717 formation can impose a steric block on kinase activity whilst structural perturbations,
718 likely emanating from sulfenylation of conserved BRSK family Cys residues within
719 critical kinase regulatory motifs, provides an additional layer of tunable regulation
720 Validation of these reversibly oxidized Cys species is also of relevance as this may
721 implicate a mechanistic role for ROS sensing in the largely obscure BRSK signaling
722 pathways that operate in different cell types, including those that impact on canonical
723 redox pathways that lead to NRF2 inactivation in cells (Tamir et al. 2020).

724

725 **Multilayered redox regulation of BRSKs**

726 The strategic positioning of Cys residues near key regulatory elements in the T-Loop
727 suggests an evolutionary adaptation for ROS-based sensing in protein kinases
728 (Beenstock, Mooshayef, and Engelberg 2016; Pearce, Komander, and Alessi 2010). Full
729 kinase activity typically requires T-Loop phosphorylation, a process further modulated
730 by mechanisms like allosteric activation in Aurora A (Eyers et al. 2003; Bayliss et al.
731 2003) and activation of CAMKs by CaM (Rellos et al. 2010). ARK family kinases, such
732 as BRSK1 and 2, are primed by phosphorylation in the T-loop of a single Thr residue by
733 the master regulatory kinase LKB1. However, our findings suggest that oxidation (or
734 reduction) of key reactive Cys residues in the kinase domains of BRSK1 /2 might
735 provide a 'dominant' regulatory oversight of enzyme output whose function in cells is
736 likely controlled by subcellular compartmentalization and/or partner protein interactions.
737
738 The ARK family of protein kinases (typified by AMPKα), share a conserved structure
739 with a notable conserved T-loop + 2 Cys residue, which is crucial for redox regulation,
740 as evidenced in AMPK and other ARKs (Byrne et al. 2020). Mutational analysis of the
741 T+2 Cys position in BRSKs confirms its critical role in supporting kinase activity.
742 Interestingly, a second Cys residue (HRD -7), co-conserved in most ARKs with the
743 exception of MELK, appears to add another regulatory dimension, with alanine
744 substitution at this site significantly reducing BRSK1 and 2 activity (Fig 4 and Supp Fig
745 4d3d). This is paralleled by the redox-sensitive Cys 130 in AMPK (Shao et al. 2014).
746 Moreover, the tendency of several ARKs to form disulfide bond-dependent dimers in
747 solution (Nayak et al. 2006; Marx et al. 2010; Cao et al. 2013) is corroborated by crystal
748 structures of MELK, MARK2, MARK3, and BRSK2 (Fig 8b), revealing asymmetric
749 dimers linked by disulfide bridges at the T-loop + 2 Cys (Marx et al. 2010; Marx et al.
750 2006; Murphy et al. 2007; Cao et al. 2013)
751
752 **BRSK-specific adaptations relevant to Cys-based signaling?**
753 BRSKs are differentiated from other ARKs and ePKs through augmentation with two
754 unique Cys residues at the HRD -1 and T-loop +9 positions, forming a novel
755 distinguishing 'CPE' motif in place of the typical APE motif found in most human protein
756 kinases. These Cys pairs facilitate intramolecular disulfide bond formation, influencing

757 kinase activity and conformation. This mechanism is reminiscent of AKT and MELK,
758 where intramolecular disulfide bonds regulate kinase activity (Murata et al. 2003; Huang
759 et al. 2003; Byrne et al. 2020; Beullens et al. 2005). Deletion of the T-loop Cys in the
760 CPE motif partially reduces BRSK1 and 2 auto-inhibition, suggesting multiple functional
761 roles for these cysteines, which is supported by our molecular dynamics (MD)
762 simulations.
763
764 Comparative evolutionary analysis indicates that approximately 1.4% of all ePKs,
765 including AKT and MELK, have cysteines at the DFG + 2 and T-loop + 2 positions
766 capable of forming similar disulfide bridges (Byrne et al. 2020; Cao et al. 2013; Huang
767 et al. 2003). MELK, despite lacking the typical HRD -7 Cys of ARKs, has compensatory
768 activation loop Cys residues that form variable disulfide bonds (Beullens et al. 2005). A
769 broader analysis across human protein kinases shows 273 unique Cys pairs capable of
770 forming disulfide bonds, suggesting a widespread regulatory mechanism in the kinome
771 (Supp. File 1). Our findings in BRSK1 and 2 highlight an extensive intramolecular
772 disulfide network, serving as a reversible switch for kinase activity and interaction
773 regulation. When considering the dominant regulative role of the T-loop available T+2
774 Cys, it is tempting to speculate that formation of intramolecular disulfides bonds with
775 adjacent cysteines may be protective against deleterious hyper-oxidized species and
776 enable rapid re-activation of the kinase after emergence from oxidative stress conditions
777 by the disulfide reductase system (Krishnan et al. 2011; Barrett et al. 1999; Chen et al.
778 2008).
779
780 The identification and characterization of unique reactive Cys residues within the kinase
781 domains of BRSK1 and 2 reveals sites of covalent-oxidative modification that may also
782 provide an underexploited opportunity to develop targeted therapeutic strategies for
783 BRSK-associated pathologies. Furthermore, mapping the spatial distribution of Cys
784 across the AMPK-related kinase family provides valuable insights into potential redox
785 hotspots that may underpin a tunable modulation of catalytic outputs with wider
786 implications for cellular signaling. As a master regulator of metabolic homeostasis,
787 AMPK activity is central to appropriate redox balance within cells (Ren and Shen 2019;

788 Choi et al. 2001; Hawley et al. 2010; Zmijewski et al. 2010; Hinchy et al. 2018; Auciello
789 et al. 2014; Shao et al. 2014), but until recently evidence of crosstalk between BRSKs
790 and redox signaling has been less clear. However, BRSKs can indirectly modulate the
791 cellular antioxidant response by orchestrating suppression of the transcription factor
792 (and master regulator/sensor of the antioxidant response), NRF2, in an mTOR-
793 dependent manner in HEK-293 cells (Tamir et al. 2020). NRF2 is targeted for
794 proteasomal degradation by its inhibitor partner, KEAP1, and under conditions of
795 elevated ROS, oxidation of sensor Cys residues in KEAP1 allows NRF2 to escape
796 ubiquitination and induce transcription of the antioxidant machinery (Baird and
797 Yamamoto 2020). Our discovery of redox regulation in BRSKs suggests that it may be
798 part of a multi-protein Cys-based 'relay' network of ROS sensitive effectors upstream of
799 NRF2, potentially constituting a new oxidative stress signaling mechanism. Uncoupling
800 the specific role of BRSKs in this pathway will be critical in illuminating BRSK1 and 2
801 physiology and their roles in neuronal function and disease and may simultaneously
802 provide an explanation for the appearance of two functional BRSK1/2 genes in
803 vertebrates.
804

Funding and additional information

Funding from N.K. (grant no: R35 GM139656) is acknowledged. P.A.E. acknowledges funding from University of Liverpool BBSRC MRC/IAA awards. A.V. acknowledges funding from ARCS Foundation. D.P.B, L.A.D., S.O.O., P.A.E. and C.E.E. also acknowledge BBSRC grants BB/S018514/1, BB/N021703/1, BB/X002780/1 and North West Cancer Research (NWCR) grant CR1208. The content is solely the responsibility of the authors and does not necessarily represent the official views of the National Institutes of Health.

Data Availability

All data generated in this study are included within the manuscript. All mass spectrometry data has been deposited at the ProteomeXchange Consortium (http://proteomecentral.proteomexchange.org) via the PRIDE partner repository with the dataset identifiers PXD044990. Source data are provided for each figure. MD simulations and associated data may be accessed from https://www.dropbox.com/sh/xtiwpjgyzxy1oz0/AACK6dS3ypzYXDih3wgKp9bla?dl=0.

Competing Interest Statement

The authors claim no competing interest.

824 **References**

825 Alessi, D. R., K. Sakamoto, and J. R. Bayascas. 2006. 'LKB1-dependent signaling
826 pathways', Annu Rev Biochem, 75: 137-63.

827 Askoxylakis, V., G. Millonig, U. Wirkner, C. Schwager, S. Rana, A. Altmann, U.
828 Haberkorn, J. Debus, S. Mueller, and P. E. Huber. 2011. 'Investigation of tumor hypoxia
829 using a two-enzyme system for in vitro generation of oxygen deficiency', Radiat. Oncol.,
830 6: 35.

831 Auciello, F. R., F. A. Ross, N. Ikematsu, and D. G. Hardie. 2014. 'Oxidative stress
832 activates AMPK in cultured cells primarily by increasing cellular AMP and/or ADP', Febs
833 Letters, 588: 3361-6.

834 Baird, L., and M. Yamamoto. 2020. 'The Molecular Mechanisms Regulating the KEAP1-
835 NRF2 Pathway', Mol Cell Biol, 40.

836 Barrett, W. C., J. P. DeGnore, S. Konig, H. M. Fales, Y. F. Keng, Z. Y. Zhang, M. B.
837 Yim, and P. B. Chock. 1999. 'Regulation of PTP1B via glutathionylation of the active site
838 cysteine 215', Biochemistry, 38: 6699-705.

839 Bayliss, R., T. Sardon, I. Vernos, and E. Conti. 2003. 'Structural basis of Aurora-A
840 activation by TPX2 at the mitotic spindle', Mol Cell, 12: 851-62.

841 Beenstock, J., N. Mooshayef, and D. Engelberg. 2016. 'How Do Protein Kinases Take a
842 Selfie (Autophosphorylate)?', Trends Biochem Sci, 41: 938-53.

843 Beullens, M., S. Vancauwenbergh, N. Morrice, R. Derua, H. Ceulemans, E. Waelkens,
844 and M. Bollen. 2005. 'Substrate specificity and activity regulation of protein kinase
845 MELK', J Biol Chem, 280: 40003-11.

846 Brandes, N., S. Schmitt, and U. Jakob. 2009. 'Thiol-based redox switches in eukaryotic
847 proteins', Antioxid Redox Signal, 11: 997-1014.

848 Bright, N. J., D. Carling, and C. Thornton. 2008. 'Investigating the regulation of brain-
849 specific kinases 1 and 2 by phosphorylation', J Biol Chem, 283: 14946-54.

850 Bright, N. J., C. Thornton, and D. Carling. 2009. 'The regulation and function of
851 mammalian AMPK-related kinases', Acta Physiol (Oxf), 196: 15-26.

852 Brooks, B. R., C. L. Brooks, 3rd, A. D. Mackerell, Jr., L. Nilsson, R. J. Petrella, B. Roux,
853 Y. Won, G. Archontis, C. Bartels, S. Boresch, A. Caflisch, L. Caves, Q. Cui, A. R.
854 Dinner, M. Feig, S. Fischer, J. Gao, M. Hodoscek, W. Im, K. Kuczera, T. Lazaridis, J.
855 Ma, V. Ovchinnikov, E. Paci, R. W. Pastor, C. B. Post, J. Z. Pu, M. Schaefer, B. Tidor,
856 R. M. Venable, H. L. Woodcock, X. Wu, W. Yang, D. M. York, and M. Karplus. 2009.
857 'CHARMM: the biomolecular simulation program', Journal of Computational Chemistry,
858 30: 1545-614.

859 Byrne, D. P., S. Shrestha, M. Galler, M. Cao, L. A. Daly, A. E. Campbell, C. E. Eyers, E.
860 A. Veal, N. Kannan, and P. A. Eyers. 2020. 'Aurora A regulation by reversible cysteine
861 oxidation reveals evolutionarily conserved redox control of Ser/Thr protein kinase
862 activity', Sci Signal, 13.

863 Byrne, D. P., M. Vonderach, S. Ferries, P. J. Brownridge, C. E. Eyers, and P. A. Eyers.
864 2016. 'cAMP-dependent protein kinase (PKA) complexes probed by complementary
865 differential scanning fluorimetry and ion mobility-mass spectrometry', Biochem J, 473:
866 3159-75.

867 Cao, L. S., J. Wang, Y. Chen, H. Deng, Z. X. Wang, and J. W. Wu. 2013. 'Structural
868 basis for the regulation of maternal embryonic leucine zipper kinase', PLoS One, 8:
869 e70031.

870 Cao, M., A. M. Day, M. Galler, H. R. Latimer, D. P. Byrne, T. W. Foy, E. Dwyer, E.
871 Bennett, J. Palmer, B. A. Morgan, P. A. Eyers, and E. A. Veal. 2023. 'A peroxiredoxin-
872 P38 MAPK scaffold increases MAPK activity by MAP3K-independent mechanisms', Mol
873 Cell.

874 Chen, Y. Y., H. M. Chu, K. T. Pan, C. H. Teng, D. L. Wang, A. H. Wang, K. H. Khoo,
875 and T. C. Meng. 2008. 'Cysteine S-nitrosylation protects protein-tyrosine phosphatase
876 1B against oxidation-induced permanent inactivation', J Biol Chem, 283: 35265-72.

877 Choi, S. L., S. J. Kim, K. T. Lee, J. Kim, J. Mu, M. J. Birnbaum, S. Soo Kim, and J. Ha.
878 2001. 'The regulation of AMP-activated protein kinase by H(2)O(2)', Biochem Biophys
879 Res Commun, 287: 92-7.

880 Corcoran, A., and T. G. Cotter. 2013. 'Redox regulation of protein kinases', Febs
881 Journal, 280: 1944-65.

882 Daly, L. A., P. J. Brownridge, M. Batie, S. Rocha, V. See, and C. E. Eyers. 2021.
883 'Oxygen-dependent changes in binding partners and post-translational modifications
884 regulate the abundance and activity of HIF-1alpha/2alpha', Sci Signal, 14.

885 Daly, Leonard A, Dominic P Byrne, Simon Perkins, Philip J Brownridge, Euan
886 McDonnell, Andrew R Jones, Patrick A Eyers, and Claire E Eyers. 2023. 'A bespoke
887 analytical workflow for the confident identification of sulfopeptides and their
888 discrimination from phosphopeptides', bioRxiv: 2023.07. 15.549150.

889 Deng, J., Y. Wang, M. Hu, J. Lin, Q. Li, C. Liu, and X. Xu. 2022. 'Deleterious Variation in
890 BR Serine/Threonine Kinase 2 Classified a Subtype of Autism', Front Mol Neurosci, 15:
891 904935.

892 Engh, R. A., and D. Bossemeyer. 2001. 'The protein kinase activity modulation sites:
893 mechanisms for cellular regulation - targets for therapeutic intervention', Adv Enzyme
894 Regul, 41: 121-49.

895 Eyers, P. A., E. Erikson, L. G. Chen, and J. L. Maller. 2003. 'A novel mechanism for
896 activation of the protein kinase Aurora A', Curr Biol, 13: 691-7.

897 Faezov, Bulat, and Jr. Roland L. Dunbrack. 2023. 'AlphaFold2 models of the active form
898 of all 437 catalytically-competent typical human kinase domains', bioRxiv:
899 2023.07.21.550125.

900 Ferries, S., S. Perkins, P. J. Brownridge, A. Campbell, P. A. Eyers, A. R. Jones, and C.
901 E. Eyers. 2017. 'Evaluation of Parameters for Confident Phosphorylation Site

902 Localization Using an Orbitrap Fusion Tribrid Mass Spectrometer', J Proteome Res, 16:
903 3448-59.

904 Fomenko, D. E., S. M. Marino, and V. N. Gladyshev. 2008. 'Functional diversity of
905 cysteine residues in proteins and unique features of catalytic redox-active cysteines in
906 thiol oxidoreductases', Mol Cells, 26: 228-35.

907 Forman, H. J., M. J. Davies, A. C. Kramer, G. Miotto, M. Zaccarin, H. Zhang, and F.
908 Ursini. 2017. 'Protein cysteine oxidation in redox signaling: Caveats on sulfenic acid
909 detection and quantification', Arch Biochem Biophys, 617: 26-37.

910 Foulkes, D. M., D. P. Byrne, W. Yeung, S. Shrestha, F. P. Bailey, S. Ferries, C. E.
911 Eyers, K. Keeshan, C. Wells, D. H. Drewry, W. J. Zuercher, N. Kannan, and P. A.
912 Eyers. 2018. 'Covalent inhibitors of EGFR family protein kinases induce degradation of
913 human Tribbles 2 (TRIB2) pseudokinase in cancer cells', Sci Signal, 11.

914 Garrido Ruiz, D., A. Sandoval-Perez, A. V. Rangarajan, E. L. Gunderson, and M. P.
915 Jacobson. 2022. 'Cysteine Oxidation in Proteins: Structure, Biophysics, and Simulation',
916 Biochemistry, 61: 2165-76.

917 Gupta, V., and K. S. Carroll. 2014. 'Sulfenic acid chemistry, detection and cellular
918 lifetime', Biochim Biophys Acta, 1840: 847-75.

919 Hawley, S. A., F. A. Ross, C. Chevtzoff, K. A. Green, A. Evans, S. Fogarty, M. C.
920 Towler, L. J. Brown, O. A. Ogunbayo, A. M. Evans, and D. G. Hardie. 2010. 'Use of cells
921 expressing gamma subunit variants to identify diverse mechanisms of AMPK activation',
922 Cell Metab, 11: 554-65.

923 Heppner, D. E., Y. M. W. Janssen-Heininger, and A. van der Vliet. 2017. 'The role of
924 sulfenic acids in cellular redox signaling: Reconciling chemical kinetics and molecular
925 detection strategies', Arch Biochem Biophys, 616: 40-46.

926 Hinchy, E. C., A. V. Gruszczyk, R. Willows, N. Navaratnam, A. R. Hall, G. Bates, T. P.
927 Bright, T. Krieg, D. Carling, and M. P. Murphy. 2018. 'Mitochondria-derived ROS
928 activate AMP-activated protein kinase (AMPK) indirectly', J Biol Chem, 293: 17208-17.

929 Hoang, D. T., O. Chernomor, A. von Haeseler, B. Q. Minh, and L. S. Vinh. 2018.
930 'UFBoot2: Improving the Ultrafast Bootstrap Approximation', Molecular Biology and
931 Evolution, 35: 518-22.

932 Huang, X., M. Begley, K. A. Morgenstern, Y. Gu, P. Rose, H. Zhao, and X. Zhu. 2003.
933 'Crystal structure of an inactive Akt2 kinase domain', Structure, 11: 21-30.

934 Huerta-Cepas, J., F. Serra, and P. Bork. 2016. 'ETE 3: Reconstruction, Analysis, and
935 Visualization of Phylogenomic Data', Molecular Biology and Evolution, 33: 1635-8.

936 Humphries, K. M., C. Juliano, and S. S. Taylor. 2002. 'Regulation of cAMP-dependent
937 protein kinase activity by glutathionylation', J Biol Chem, 277: 43505-11.

938 Jarvis, R. M., S. M. Hughes, and E. C. Ledgerwood. 2012. 'Peroxiredoxin 1 functions as
939 a signal peroxidase to receive, transduce, and transmit peroxide signals in mammalian
940 cells', Free Radic Biol Med, 53: 1522-30.

941 Jo, S., X. Cheng, S. M. Islam, L. Huang, H. Rui, A. Zhu, H. S. Lee, Y. Qi, W. Han, K.
942 Vanommeslaeghe, A. D. MacKerell, Jr., B. Roux, and W. Im. 2014. 'CHARMM-GUI PDB
943 manipulator for advanced modeling and simulations of proteins containing nonstandard
944 residues', Adv Protein Chem Struct Biol, 96: 235-65.

945 Jumper, J., R. Evans, A. Pritzel, T. Green, M. Figurnov, O. Ronneberger, K.
946 Tunyasuvunakool, R. Bates, A. Zidek, A. Potapenko, A. Bridgland, C. Meyer, S. A. A.
947 Kohl, A. J. Ballard, A. Cowie, B. Romera-Paredes, S. Nikolov, R. Jain, J. Adler, T. Back,
948 S. Petersen, D. Reiman, E. Clancy, M. Zielinski, M. Steinegger, M. Pacholska, T.
949 Berghammer, S. Bodenstein, D. Silver, O. Vinyals, A. W. Senior, K. Kavukcuoglu, P.
950 Kohli, and D. Hassabis. 2021. 'Highly accurate protein structure prediction with
951 AlphaFold', Nature, 596: 583-89.

952 Kalyaanamoorthy, S., B. Q. Minh, T. K. F. Wong, A. von Haeseler, and L. S. Jermiin.
953 2017. 'ModelFinder: fast model selection for accurate phylogenetic estimates', Nat
954 Methods, 14: 587-89.

955 Kishi, M., Y. A. Pan, J. G. Crump, and J. R. Sanes. 2005. 'Mammalian SAD kinases are
956 required for neuronal polarization', Science, 307: 929-32.

957 Krishnan, N., C. Fu, D. J. Pappin, and N. K. Tonks. 2011. 'H2S-Induced sulfhydration of
958 the phosphatase PTP1B and its role in the endoplasmic reticulum stress response', Sci
959 Signal, 4: ra86.

960 Lee, J., X. Cheng, J. M. Swails, M. S. Yeom, P. K. Eastman, J. A. Lemkul, S. Wei, J.
961 Buckner, J. C. Jeong, Y. Qi, S. Jo, V. S. Pande, D. A. Case, C. L. Brooks, 3rd, A. D.
962 MacKerell, Jr., J. B. Klauda, and W. Im. 2016. 'CHARMM-GUI Input Generator for
963 NAMD, GROMACS, AMBER, OpenMM, and CHARMM/OpenMM Simulations Using the
964 CHARMM36 Additive Force Field', J Chem Theory Comput, 12: 405-13.

965 Lennicke, C., J. Rahn, R. Lichtenfels, L. A. Wessjohann, and B. Seliger. 2015.
966 'Hydrogen peroxide - production, fate and role in redox signaling of tumor cells', Cell
967 Commun Signal, 13: 39.

968 Li, R., M. He, B. Wu, P. Zhang, Q. Zhang, and Y. Chen. 2020. 'SAD-B modulates
969 epileptic seizure by regulating AMPA receptors in patients with temporal lobe epilepsy
970 and in the PTZ-induced epileptic model', Braz J Med Biol Res, 53: e9175.

971 Lizcano, J. M., O. Goransson, R. Toth, M. Deak, N. A. Morrice, J. Boudeau, S. A.
972 Hawley, L. Udd, T. P. Makela, D. G. Hardie, and D. R. Alessi. 2004. 'LKB1 is a master
973 kinase that activates 13 kinases of the AMPK subfamily, including MARK/PAR-1',
974 EMBO J, 23: 833-43.

975 Manning, G., D. B. Whyte, R. Martinez, T. Hunter, and S. Sudarsanam. 2002. 'The
976 protein kinase complement of the human genome', Science, 298: 1912-34.

977 Marx, A., C. Nugoor, J. Muller, S. Panneerselvam, T. Timm, M. Bilang, E. Mylonas, D. I.
978 Svergun, E. M. Mandelkow, and E. Mandelkow. 2006. 'Structural variations in the
979 catalytic and ubiquitin-associated domains of microtubule-associated
980 protein/microtubule affinity regulating kinase (MARK) 1 and MARK2', J Biol Chem, 281:
981 27586-99.

982 Marx, A., C. Nugoor, S. Panneerselvam, and E. Mandelkow. 2010. 'Structure and
983 function of polarity-inducing kinase family MARK/Par-1 within the branch of AMPK/Snf1-
984 related kinases', FASEB J, 24: 1637-48.

985 Michaud-Agrawal, N., E. J. Denning, T. B. Woolf, and O. Beckstein. 2011. 'MDAnalysis:
986 a toolkit for the analysis of molecular dynamics simulations', Journal of Computational
987 Chemistry, 32: 2319-27.

988 Minh, B. Q., H. A. Schmidt, O. Chernomor, D. Schrempf, M. D. Woodhams, A. von
989 Haeseler, and R. Lanfear. 2020. 'IQ-TREE 2: New Models and Efficient Methods for
990 Phylogenetic Inference in the Genomic Era', Molecular Biology and Evolution, 37: 1530-
991 34.

992 Mohanty, S., K. Oruganty, A. Kwon, D. P. Byrne, S. Ferries, Z. Ruan, L. E. Hanold, S.
993 Katiyar, E. J. Kennedy, P. A. Eyers, and N. Kannan. 2016. 'Hydrophobic Core Variations
994 Provide a Structural Framework for Tyrosine Kinase Evolution and Functional
995 Specialization', PLoS Genet, 12: e1005885.

996 Morshed, Nader, Meelim J Lee, Felicia H Rodriguez, Douglas A Lauffenburger, Diego
997 Mastroeni, and Forest M White. 2021. 'Quantitative phosphoproteomics uncovers
998 dysregulated kinase networks in Alzheimer's disease', Nature Aging, 1: 550-65.

999 Mueller, S., G. Millonig, and G. Waite. 2009. 'The GOX/CAT system: A novel enzymatic
1000 method to independently control hydrogen peroxide and hypoxia in cell culture', Adv.
1001 Med. Sci., 54: 121–135.

1002 Murata, H., Y. Ihara, H. Nakamura, J. Yodoi, K. Sumikawa, and T. Kondo. 2003.
1003 'Glutaredoxin exerts an antiapoptotic effect by regulating the redox state of Akt', J Biol
1004 Chem, 278: 50226-33.

1005 Murphy, J. M., D. M. Korzhnev, D. F. Ceccarelli, D. J. Briant, A. Zarrine-Afsar, F.
1006 Sicheri, L. E. Kay, and T. Pawson. 2007. 'Conformational instability of the MARK3 UBA
1007 domain compromises ubiquitin recognition and promotes interaction with the adjacent
1008 kinase domain', Proc Natl Acad Sci U S A, 104: 14336-41.

1009 Murphy, J. M., Q. Zhang, S. N. Young, M. L. Reese, F. P. Bailey, P. A. Eyers, D.
1010 Ungureanu, H. Hammaren, O. Silvennoinen, L. N. Varghese, K. Chen, A. Tripaydonis,
1011 N. Jura, K. Fukuda, J. Qin, Z. Nimchuk, M. B. Mudgett, S. Elowe, C. L. Gee, L. Liu, R. J.
1012 Daly, G. Manning, J. J. Babon, and I. S. Lucet. 2014. 'A robust methodology to
1013 subclassify pseudokinases based on their nucleotide-binding properties', Biochem J,
1014 457: 323-34.

1015 Nayak, V., K. Zhao, A. Wyce, M. F. Schwartz, W. S. Lo, S. L. Berger, and R.
1016 Marmorstein. 2006. 'Structure and dimerization of the kinase domain from yeast Snf1, a
1017 member of the Snf1/AMPK protein family', Structure, 14: 477-85.

1018 Nakanishi, K., H. Niida, H. Tabata, T. Ito, Y. Hori, M. Hattori, Y. Johmura, C. Yamada, T.
1019 Ueda, K. Takeuchi, K. Yamada, K. Nagata, N. Wakamatsu, M. Kishi, Y. A. Pan, S.
1020 Ugawa, S. Shimada, J. R. Sanes, Y. Higashi, and M. Nakanishi. 2019. 'Isozyme-
1021 Specific Role of SAD-A in Neuronal Migration During Development of Cerebral Cortex',
1022 Cerebral Cortex, 29: 3738-51.

1023 Nayak, V., K. Zhao, A. Wyce, M. F. Schwartz, W. S. Lo, S. L. Berger, and R.
1024 Marmorstein. 2006. 'Structure and dimerization of the kinase domain from yeast Snf1, a
1025 member of the Snf1/AMPK protein family', Structure, 14: 477-85.

1026 Neuwald, A. F. 2009. 'Rapid detection, classification and accurate alignment of up to a
1027 million or more related protein sequences', Bioinformatics, 25: 1869-75.

1028 Nie, J., C. Sun, O. Faruque, G. Ye, J. Li, Q. Liang, Z. Chang, W. Yang, X. Han, and Y.
1029 Shi. 2012. 'Synapses of amphids defective (SAD-A) kinase promotes glucose-
1030 stimulated insulin secretion through activation of p21-activated kinase (PAK1) in
1031 pancreatic beta-Cells', J Biol Chem, 287: 26435-44.

1032 Nolen, B., S. Taylor, and G. Ghosh. 2004. 'Regulation of protein kinases; controlling
1033 activity through activation segment conformation', Mol Cell, 15: 661-75.

1034 Pearce, L. R., D. Komander, and D. R. Alessi. 2010. 'The nuts and bolts of AGC protein
1035 kinases', Nat Rev Mol Cell Biol, 11: 9-22.

1036 Perkins, D. N., D. J. Pappin, D. M. Creasy, and J. S. Cottrell. 1999. 'Probability-based
1037 protein identification by searching sequence databases using mass spectrometry data',
1038 Electrophoresis, 20: 3551-67.

1039 Poole, L. B. 2015. 'The basics of thiols and cysteines in redox biology and chemistry',
1040 Free Radic Biol Med, 80: 148-57.

1041 Rellos, P., A. C. Pike, F. H. Niesen, E. Salah, W. H. Lee, F. von Delft, and S. Knapp.
1042 2010. 'Structure of the CaMKIIdelta/calmodulin complex reveals the molecular
1043 mechanism of CaMKII kinase activation', PLoS Biol, 8: e1000426.

1044 Ren, Y., and H. M. Shen. 2019. 'Critical role of AMPK in redox regulation under glucose
1045 starvation', Redox Biol, 25: 101154.

1046 Rhee, S. G., S. W. Kang, W. Jeong, T. S. Chang, K. S. Yang, and H. A. Woo. 2005.
1047 'Intracellular messenger function of hydrogen peroxide and its regulation by
1048 peroxiredoxins', Curr Opin Cell Biol, 17: 183-9.

1049 Saiyin, H., N. Na, X. Han, Y. Fang, Y. Wu, W. Lou, and X. Yang. 2017. 'BRSK2 induced
1050 by nutrient deprivation promotes Akt activity in pancreatic cancer via downregulation of
1051 mTOR activity', Oncotarget, 8: 44669-81.

1052 Salmeen, A., J. N. Andersen, M. P. Myers, T. C. Meng, J. A. Hinks, N. K. Tonks, and D.
1053 Barford. 2003. 'Redox regulation of protein tyrosine phosphatase 1B involves a
1054 sulphenyl-amide intermediate', Nature, 423: 769-73.

1055 Schieber, M., and N. S. Chandel. 2014. 'ROS function in redox signaling and oxidative
1056 stress', Curr Biol, 24: R453-62.

1057 Schrodinger, LLC. 2015. "The PyMOL Molecular Graphics System, Version 1.8." In.

1058 Shao, D., S. Oka, T. Liu, P. Zhai, T. Ago, S. Sciarretta, H. Li, and J. Sadoshima. 2014.
1059 'A redox-dependent mechanism for regulation of AMPK activation by Thioredoxin1
1060 during energy starvation', Cell Metab, 19: 232-45.

1061 Shirwany, N. A., and M. H. Zou. 2014. 'AMPK: a cellular metabolic and redox sensor. A
1062 minireview', Front Biosci (Landmark Ed), 19: 447-74.

1063 Soylu, I., and S. M. Marino. 2016. 'Cy-preds: An algorithm and a web service for the
1064 analysis and prediction of cysteine reactivity', Proteins, 84: 278-91.

1065 Su, Z., J. G. Burchfield, P. Yang, S. J. Humphrey, G. Yang, D. Francis, S. Yasmin, S. Y.
1066 Shin, D. M. Norris, A. L. Kearney, M. A. Astore, J. Scavuzzo, K. H. Fisher-Wellman, Q.
1067 P. Wang, B. L. Parker, G. G. Neely, F. Vafaee, J. Chiu, R. Yeo, P. J. Hogg, D. J.
1068 Fazakerley, L. K. Nguyen, S. Kuyucak, and D. E. James. 2019. 'Global redox proteome
1069 and phosphoproteome analysis reveals redox switch in Akt', Nat Commun, 10: 5486.

1070 Tamir, T. Y., D. H. Drewry, C. Wells, M. B. Major, and A. D. Axtman. 2020. 'PKIS deep
1071 dive yields a chemical starting point for dark kinases and a cell active BRSK2 inhibitor',
1072 Sci Rep, 10: 15826.

1073 Tamir, T. Y., B. M. Bowman, M. J. Agajanian, D. Goldfarb, T. P. Schrank, T. Stohrer, A.
1074 E. Hale, P. F. Siesser, S. J. Weir, R. M. Murphy, K. M. LaPak, B. E. Weissman, N. J.
1075 Moorman, and M. B. Major. 2020. 'Gain-of-function genetic screen of the kinome
1076 reveals BRSK2 as an inhibitor of the NRF2 transcription factor', J Cell Sci, 133.

1077 Truong, T. H., and K. S. Carroll. 2013. 'Redox regulation of protein kinases', Crit Rev
1078 Biochem Mol Biol, 48: 332-56.

1079 Truong, T. H., P. M.-U. Ung, P. B. Palde, C. E. Paulsen, A. Schlessinger, and K. S.
1080 Carroll. 2016. 'Molecular basis for redox activation of epidermal growth factor receptor
1081 kinase', Cell Chem. Biol., 23: 837–848.

1082 Tsuchiya, Y., D. P. Byrne, S. G. Burgess, J. Bormann, J. Bakovic, Y. Huang, A.
1083 Zhyvoloup, B. Y. K. Yu, S. Peak-Chew, T. Tran, F. Bellany, A. B. Tabor, A. E. Chan, L.
1084 Guruprasad, O. Garifulin, V. Filonenko, M. Vonderach, S. Ferries, C. E. Eyers, J.
1085 Carroll, M. Skehel, R. Bayliss, P. A. Eyers, and I. Gout. 2020. 'Covalent Aurora A
1086 regulation by the metabolic integrator coenzyme A', Redox Biol, 28: 101318.

1087 UniProt, Consortium. 2023. 'UniProt: the Universal Protein Knowledgebase in 2023',
1088 Nucleic Acids Res, 51: D523-D31.

1089 Van Der Spoel, D., E. Lindahl, B. Hess, G. Groenhof, A. E. Mark, and H. J. Berendsen.
1090 2005. 'GROMACS: fast, flexible, and free', Journal of Computational Chemistry, 26:
1091 1701-18.

1092 van Montfort, R. L., M. Congreve, D. Tisi, R. Carr, and H. Jhoti. 2003. 'Oxidation state of
1093 the active-site cysteine in protein tyrosine phosphatase 1B', Nature, 423: 773-7.

1094 Venkat, A., G. Watterson, D. P. Byrne, B. O'Boyle, S. Shrestha, N. Gravel, E. E.
1095 Fairweather, L. A. Daly, C. Bunn, W. Yeung, I. Aggarwal, S. Katiyar, C. E. Eyers, P. A.
1096 Eyers, and N. Kannan. 2023. 'Mechanistic and evolutionary insights into isoform-specific
1097 'supercharging' in DCLK family kinases', bioRxiv.

1098 Wani, R., J. Qian, L. Yin, E. Bechtold, S. B. King, L. B. Poole, E. Paek, A. W. Tsang,
1099 and C. M. Furdui. 2011. 'Isoform-specific regulation of Akt by PDGF-induced reactive
1100 oxygen species', Proc Natl Acad Sci U S A, 108: 10550-5.

Weisner, J., R. Gontla, L. van der Westhuizen, S. Oeck, J. Ketzer, P. Janning, A. Richters, T. Muhlenberg, Z. Fang, A. Taher, V. Jendrossek, S. C. Pelly, S. Bauer, W. A. van Otterlo, and D. Rauh. 2015. 'Covalent-Allosteric Kinase Inhibitors', Angew Chem Int Ed Engl, 54: 10313-6.

Wu, J. X., Y. S. Cheng, J. Wang, L. Chen, M. Ding, and J. W. Wu. 2015. 'Structural insight into the mechanism of synergistic autoinhibition of SAD kinases', Nat Commun, 6: 8953.

Xiao, H., M. P. Jedrychowski, D. K. Schweppe, E. L. Huttlin, Q. Yu, D. E. Heppner, J. Li, J. Long, E. L. Mills, J. Szpyt, Z. He, G. Du, R. Garrity, A. Reddy, L. P. Vaites, J. A. Paulo, T. Zhang, N. S. Gray, S. P. Gygi, and E. T. Chouchani. 2020. 'A Quantitative Tissue-Specific Landscape of Protein Redox Regulation during Aging', Cell, 180: 968-83 e24.

Yeung, W., A. Kwon, R. Taujale, C. Bunn, A. Venkat, and N. Kannan. 2021. 'Evolution of Functional Diversity in the Holozoan Tyrosine Kinome', Molecular Biology and Evolution, 38: 5625-39.

Yoshida, H., and M. Goedert. 2012. 'Phosphorylation of microtubule-associated protein tau by AMPK-related kinases', J Neurochem, 120: 165-76.

Zmijewski, J. W., S. Banerjee, H. Bae, A. Friggeri, E. R. Lazarowski, and E. Abraham. 2010. 'Exposure to hydrogen peroxide induces oxidation and activation of AMP-activated protein kinase', J Biol Chem, 285: 33154-64.

1137

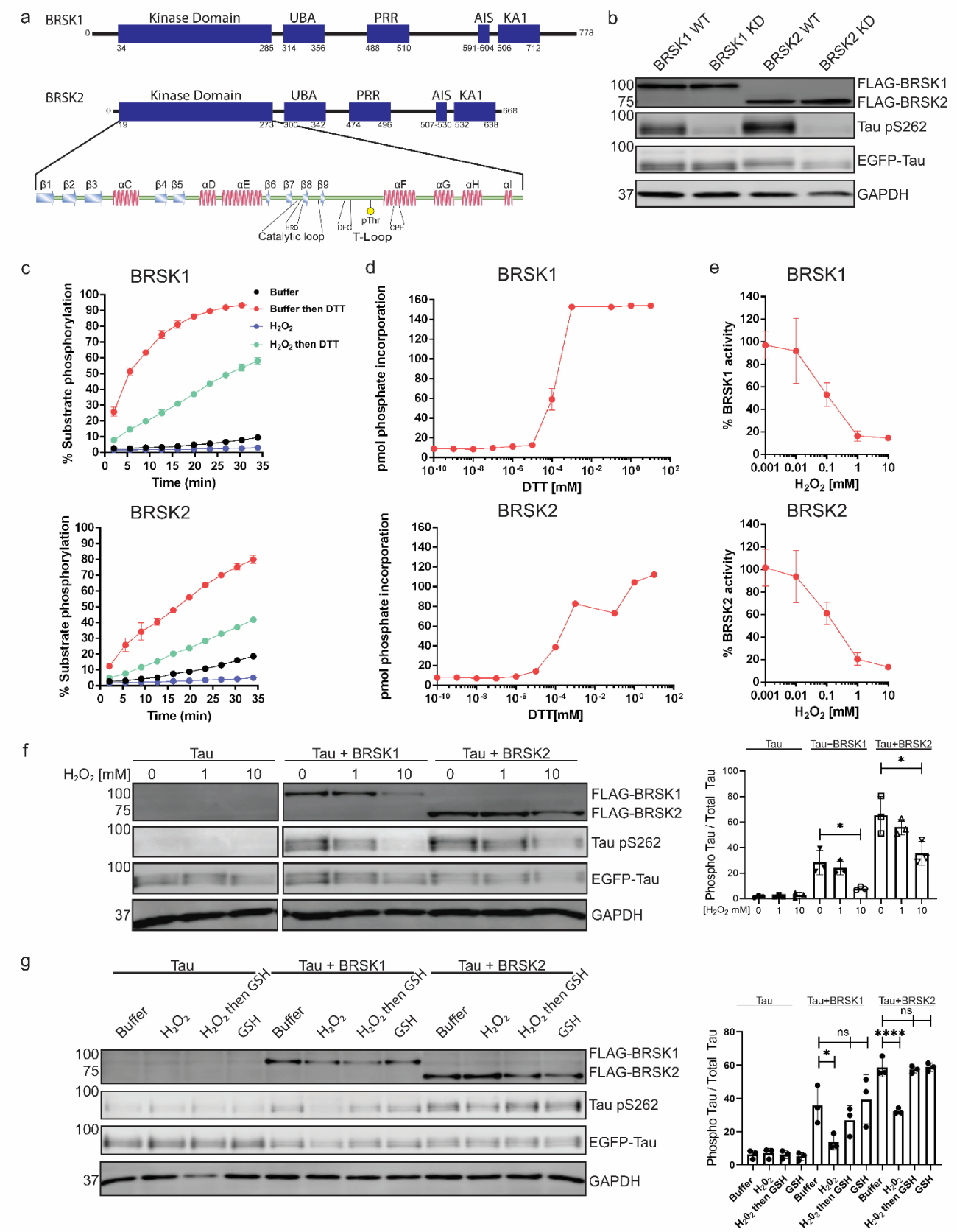
a
BRSK1
Kinase Domain
UBA
PRR
AIS
KA1
BRSK2
Catalytic loop
T-Loop
b
BRSK1 WT
BRSK1 KD
BRSK2 WT
BRSK2 KD
FLAG-BRSK1
FLAG-BRSK2
Tau pS262
EGFP-Tau
GAPDH
c
BRSK1
Buffer
Buffer then DTT
H2O2
H2O2 then DTT
% Substrate phosphorylation
Time (min)
BRSK2
d
pmol phosphate incorporation
DTT [mM]
e
% BRSK1 activity
% BRSK2 activity
H2O2 [mM]
f
Tau
Tau + BRSK1
Tau + BRSK2
H2O2 [mM]
Phospho Tau / Total Tau
g
Buffer
H2O2
H2O2 then GSH
GSH
ns
****

1138 Figure 1: BRSK1/2 are redox sensitive. (a) Schematic representation of BRSK domain
1139 architecture, including Kinase domain, Ubiquitin Associated (UBA) domain,
1140 Proline-Rich Region (PRR), Kinase Associated Domain(KA1), and Autoinhibitory
1141 Sequence (AIS). (b) Immunoblotting showing BRSK dependent phosphorylation
1142 of Tau at Ser262 (pS262), from lysates of HEK-293T cells overexpressing full-
1143 length FLAG-BRSK1 or 2 (wild type [WT] or kinase dead [KD]) and EGFP-Tau.
1144 (c) Real time phosphorylation of fluorescent AMARA peptide by full length
1145 BRSK1 and 2 (200 ng) purified from Sf21 cells. BRSK proteins were incubated
1146 with buffer or 1 mM H_2O_2 for 10 mins, reactions were then initiated with the
1147 addition of ATP and peptide substrate in the presence (where indicated) of 10
1148 mM DTT. Dose response curves for (d) DTT and (e) H_2O_2 with 200 ng full-length
1149 BRSK1 and BRSK2. All kinases assays are shown as mean and SD of three
1150 experiments. (f) Immunoblott (left) of pS262 in transiently co-transfected HEK-
1151 293T cells incubated with the indicated concentration of H_2O_2 for 10 mins. Signal
1152 density for phospho Tau S262 and total Tau (GFP) was obtained using
1153 ImageStudio software (Licor) and results from at least 3 biological replicates
1154 were anaylzed with Graphpad Prism software using one way anova to determine
1155 significance. Data shown is mean and SE. (g) Representative immunoblot (left)
1156 of transiently co-transfected HEK-293T cells treated with 10 mM H_2O_2 for 10
1157 mins before the addition of 20 mM GSH. Whole cell lysates were harvested after
1158 a further 15 mins. Normalized densitometry of Tau pS262 signal (right) was
1159 calculated from 3 independent experiments. Data shown is mean and SD. * = $P < 0.05$, **= $P < 0.01$, ***= $P < 0.001$.

1161

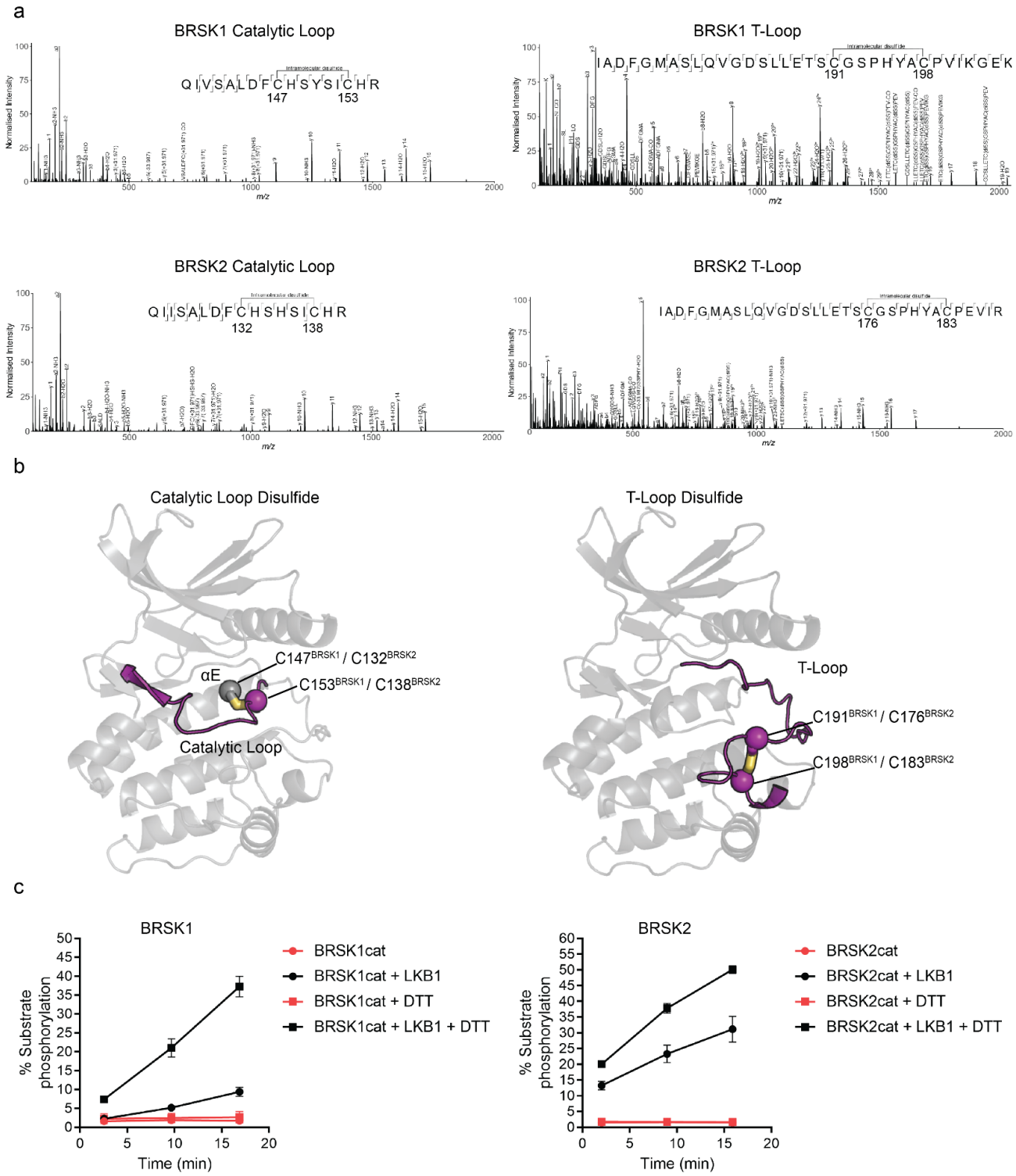
a
BRSK1 Catalytic Loop
Q I V S A L D F C H S Y S I C H R
147
153
BRSK1 T-Loop
I A D F G M A S L Q V G D S L L E T S C G S P H Y A C P V I K G E K
191
198
BRSK2 Catalytic Loop
Q I I S A L D F C H S H S I C H R
132
138
BRSK2 T-Loop
I A D F G M A S L Q V G D S L L E T S C G S P H Y A C P E V I R
176
183
Normalised Intensity
m/z
b
Catalytic Loop Disulfide
αE
C147BRSK1 / C132BRSK2
C153BRSK1 / C138BRSK2
Catalytic Loop
T-Loop Disulfide
T-Loop
C191BRSK1 / C176BRSK2
C198BRSK1 / C183BRSK2
c
BRSK1
BRSK1cat
BRSK1cat + LKB1
BRSK1cat + DTT
BRSK1cat + LKB1 + DTT
% Substrate phosphorylation
Time (min)
BRSK2
BRSK2cat
BRSK2cat + LKB1
BRSK2cat + DTT
BRSK2cat + LKB1 + DTT
% Substrate phosphorylation
Time (min)

1162 Figure 2: Intramolecular disulfide bonds form in the kinase domains of BRSK1 and 2. (a)
1163 Full length BRSK1 and 2 were affinity-purified from HEK-293T cells and
1164 subjected to LC-MS/MS analysis. LC-MS/MS spectrum mapping revealed
1165 disulfide bridges formation between $C147^{BRSK1}$ - $C153^{BRSK1}$, $C191^{BRSK1}$ -
1166 $C198^{BRSK1}$, $C132^{BRSK2}$ - $C138^{BRSK2}$, and $C176^{BRSK2}$ - $C183^{BRSK2}$. Peptide
1167 coverage was 74 and 78 % for BRSK1 and BRSK2 respectively. (b) Alphafold
1168 structures demonstrating the location of disulfide bonds within the kinase
1169 domains of BRSK1 and BRSK2. (c) Real time phosphorylation of fluorescent
1170 AMARA peptide by the kinase domains of BRSK1 and 2 (100 ng) purified from
1171 *E.coli* . BRSK1 (29-358) and BRSK2 (14-341) were activated by incubation with
1172 LKB1 and assayed in the presence or absence of 1 mM DTT.

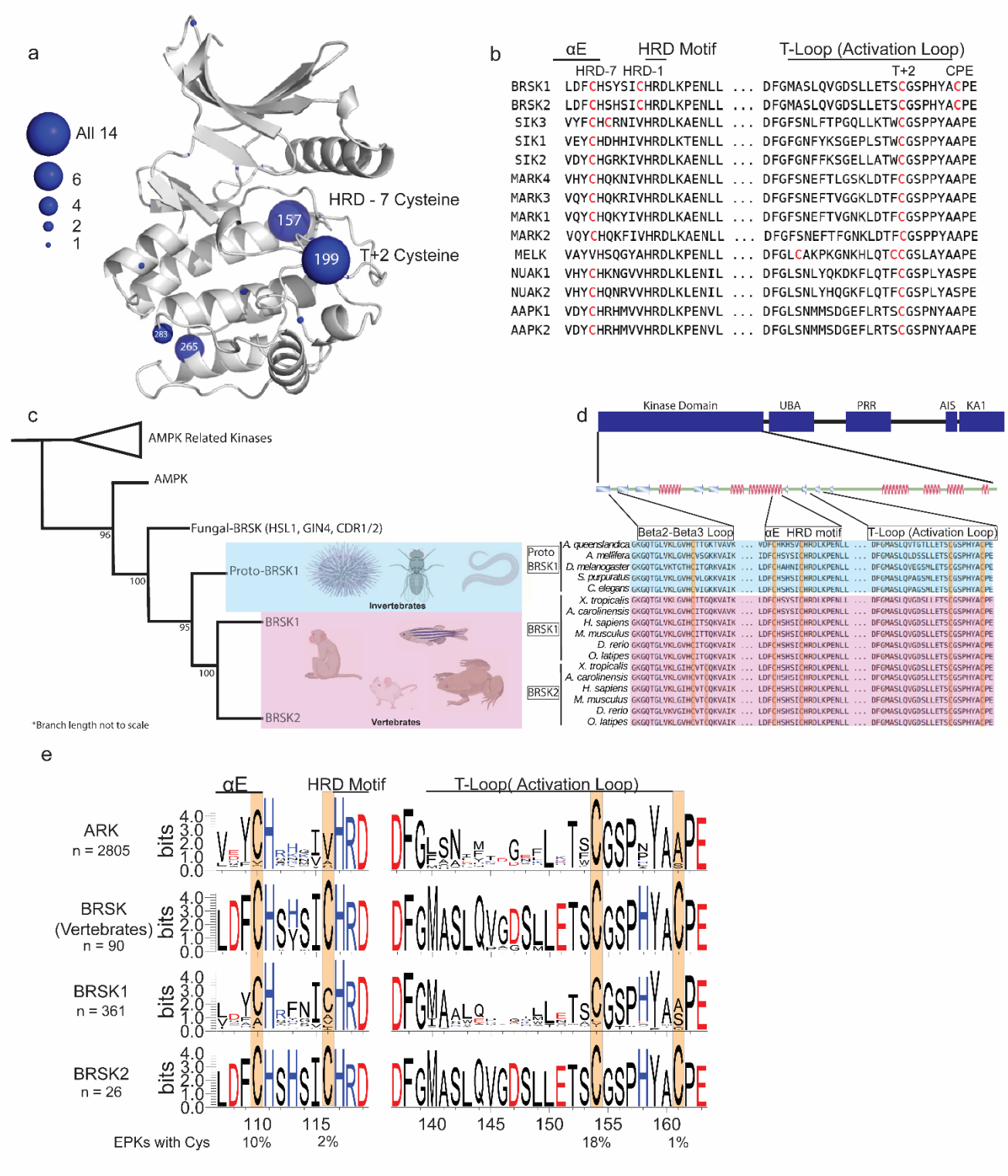

Figure 3: Cysteine pairs are highly conserved within the activation segments of BRSKs. (a) Mapping of Cys residues (spheres) in the kinase domains of human ARK family members. Numbers represent the corresponding amino acid position in

PKA. Sphere size is proportional to the number of ARKs that contain a Cys at a specific site. (b) Activation segment sequence alignment of the 14 human ARKs. (c) Phylogenetic analysis showing divergence and grouping of BRSKs sub-families in different taxonomic groups. Bootstrap values are included for each clade. (d) Sequence alignment of the kinase domains of invertebrate and vertebrate BRSKs. (e) Analysis of relative amino acid conservation in ARKs and BRSKs, centered on the HRD containing catalytic loop, and the T-loop (between the DFG and APE motifs). Data is presented as HMM (hidden Markov models) Sequence Logos. The % of ePKs that possess a specific Cys is shown at the bottom.

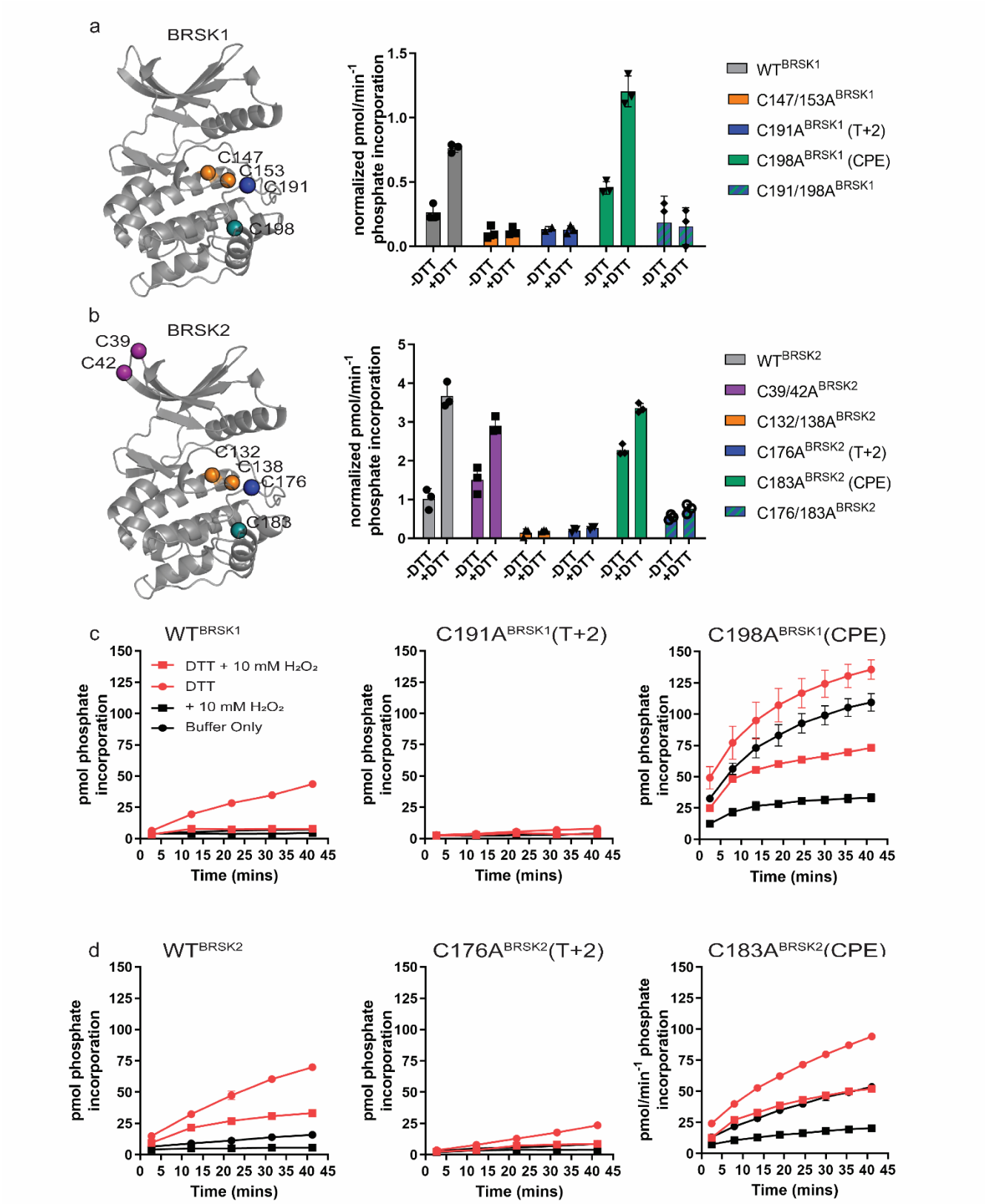
a
BRSK1
C147
C153
C191
C198
normalized pmol/min-1 phosphate incorporation
WTBRSK1
C147/153ABRSK1
C191ABRSK1 (T+2)
C198ABRSK1 (CPE)
C191/198ABRSK1
-DTT
+DTT
b
BRSK2
C39
C42
C132
C138
C176
C183
WTBRSK2
C39/42ABRSK2
C132/138ABRSK2
C176ABRSK2 (T+2)
C183ABRSK2 (CPE)
C176/183ABRSK2
c
WTBRSK1
C191ABRSK1(T+2)
C198ABRSK1(CPE)
DTT + 10 mM H2O2
DTT
+ 10 mM H2O2
Buffer Only
pmol phosphate incorporation
Time (mins)
d
WTBRSK2
C176ABRSK2(T+2)
C183ABRSK2(CPE)
pmol/min-1 phosphate incorporation

1187

Figure 4: Cysteine residues within the kinase domain fine-tune BRSK activity. In vitro kinase assays (right panels) showing normalized rates of peptide phosphorylation by WT and Cys-to-Ala variants of (a) BRSK1 and (b) BRSK2. 100 ng of LKB1 activated BRSK kinase domain was assayed in the presence or absence of 1 mM DTT. The positions of mutated Cys residues are modelled on the kinase domain as coloured spheres (left panel). Real time in vitro assays using (c) 50 ng BRSK1 and (d) 20 ng BRSK2. LKB1-activated BRSK proteins were incubated on ice in the presence or absence of 250 µM DTT for 30 mins. Assays were initiated by the addition of ATP and fluorescent peptide substrate in the presence or absence of 1 mM H_2O_2. All data is mean and SD of 3 experiments and activities are normalized to LKB1-phosphorylated BRSK signal (Supp Fig 4 b).

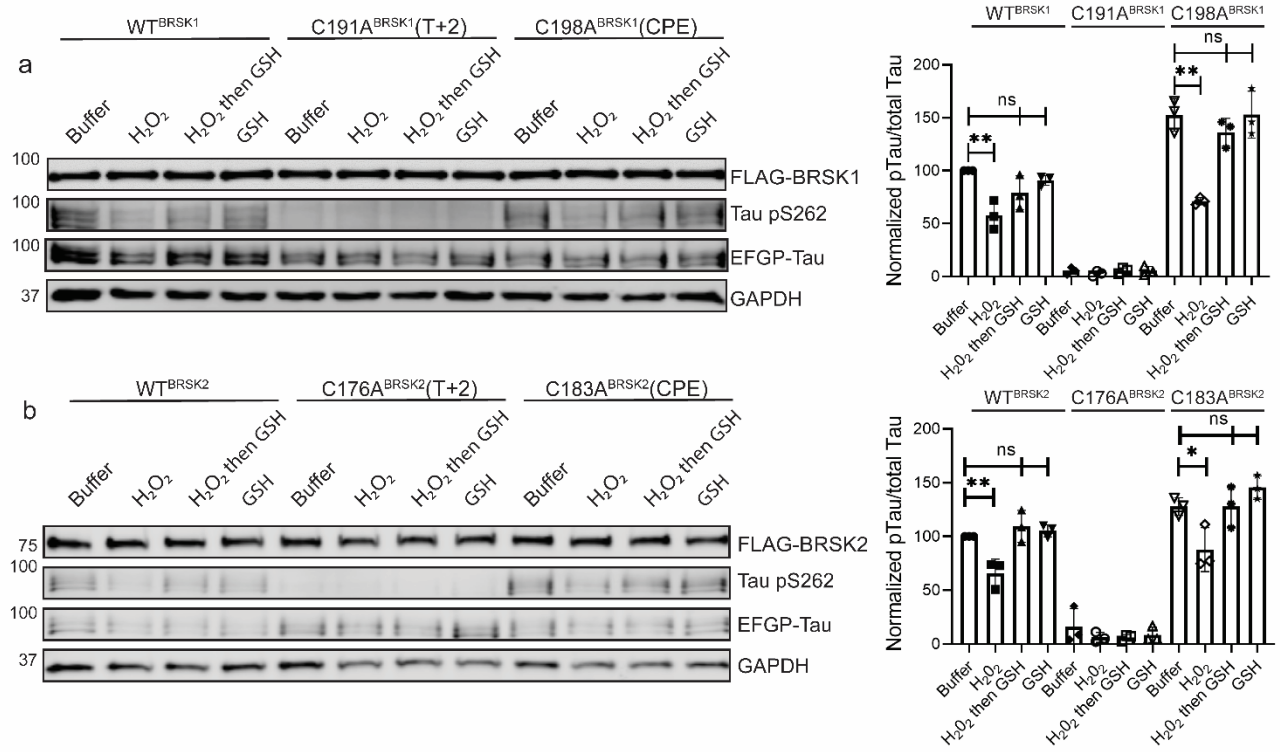

Figure 5: Impact of T-Loop and CPE Cys-to-Ala mutations on BRSK redox sensitivity in a cellular EGFP-Tau HEK-293T co-expression system. Representative immunoblot of EGFP-Tau co-expressed with WT and Cys-to-Ala mutants of (a) BRSK1 and (b) BRSK2 (left panels). Transiently transfected HEK-293T cells were treated with or without 10 mM H_2O_2 for 10 mins before the addition of 20

mM GSH. Whole cell lysates were harvested after a further 15 mins. Signal density for phospho Tau S262 and total Tau (GFP) was obtained using ImageStudio software (Licor) and results from at least 3 biological replicates were anaylzed with Graphpad Prism software using one way anova to determine significance (right panels). Data shown is mean and SE. All values are normalized to Tau pS262 signals from control (buffer only treatment) WT BRSK and Tau co-transfections. Data shown is mean and SD. * = P < 0.05, **= P < 0.01, ***= P < 0.001.

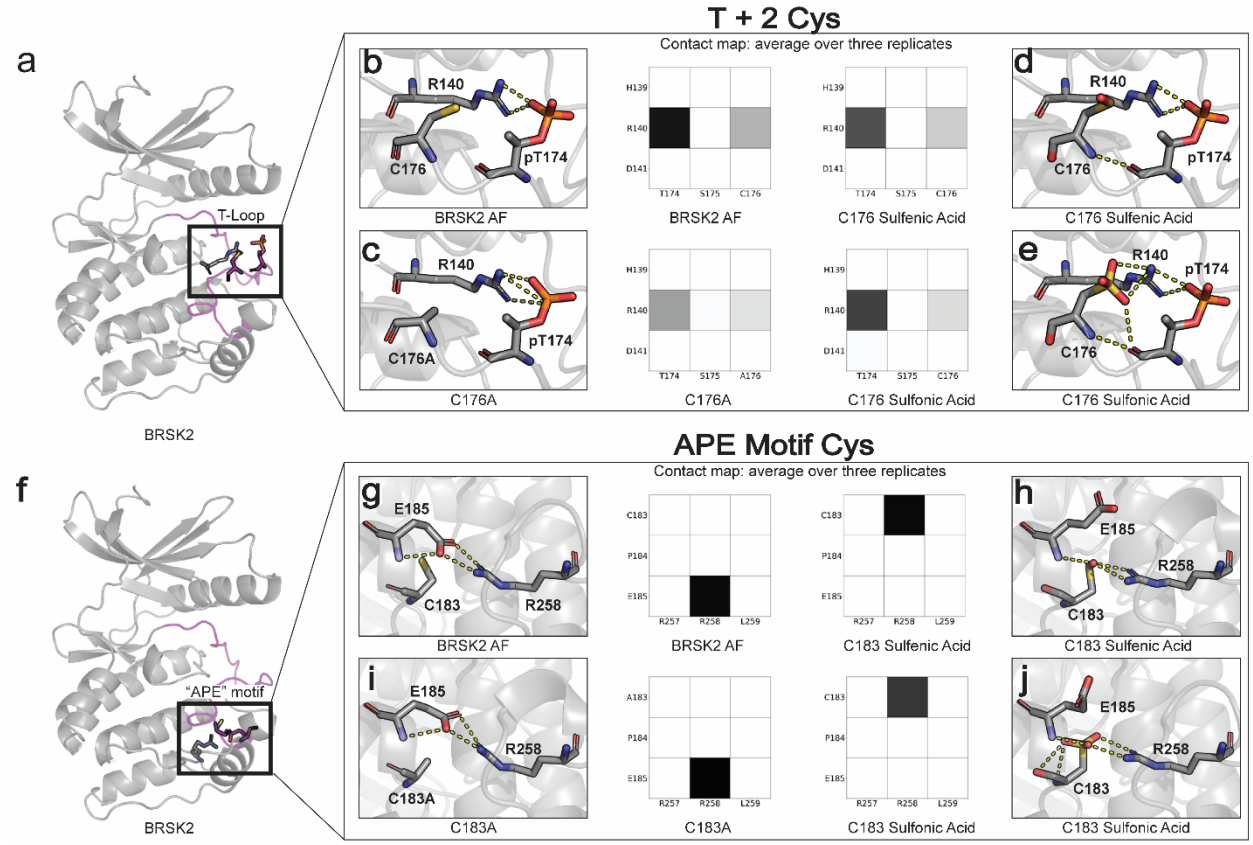

Figure 6: Oxidative cysteine modifications alter critical structural interactions required for BRSK allosteric regulation. Three replicates of 100 ns GROMACS molecular dynamics simulations were performed to evaluate the effects of cysteine mutation and oxidation. Salt bridge disruption was analyzed by generating contact maps representing the percentage of the simulation time in which residues were within appropriate distance (3 Angstroms). (a) T+2 Cys is located in proximity to the activation loop threonine in the T loop. (b-e) Evaluation of pT174-R140 salt bridge formation in wild type, C176A, and oxidized C176 BRSK2. (f) Location of CPE salt bridge within BRSK2. (g-j) Evaluation of E185-R258 salt bridge formation in wild type, C183A, and oxidized C183 BRSK2.

1228

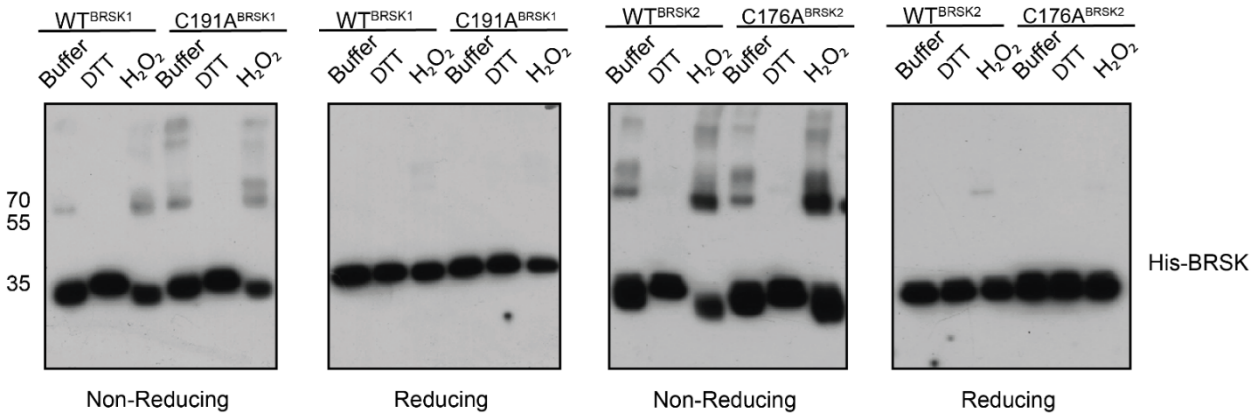

1229

1230 Figure 7: BRSK1/2 form limited disulfide-mediated multimers. Western blot analysis of
1231 BRSK1/2 kinase domain purified from *E. coli* and incubated with buffer, H_2O_2, or
1232 DTT and subjected to non-reducing or reducing PAGE to evalute the formation of
1233 intramolecular disulfide bonds.
1234

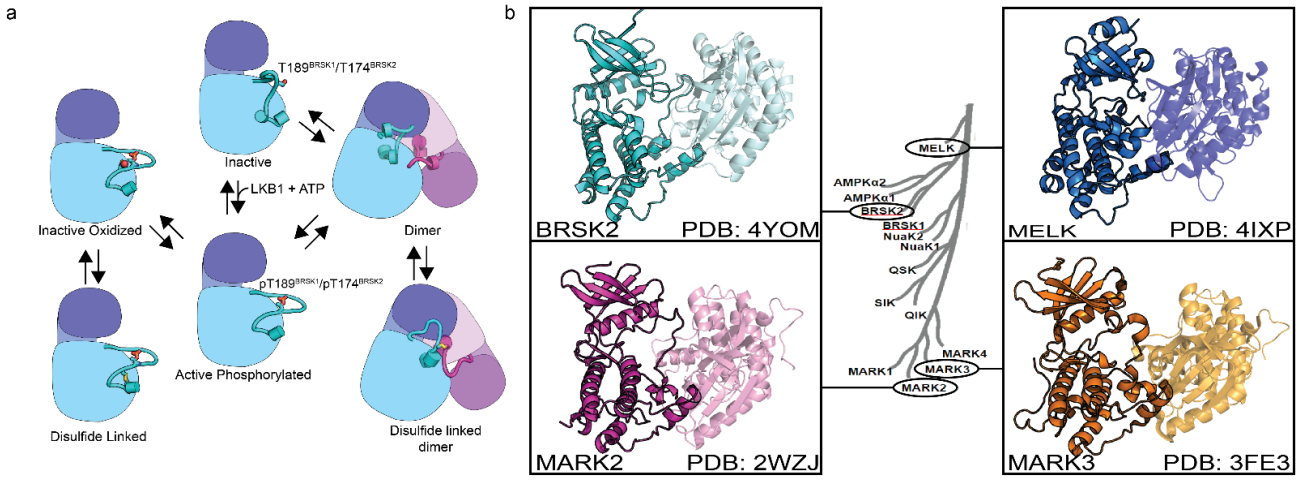

1235

1236 Figure 8: (a) Model of BRSK1/2 regulation. Schematic diagram demonstrating ways in
1237 which residues within BRSK kinases permit fine-tuning of catalytic activity
1238 through a variety of oxidative modifications, potentially including inter and
1239 intramolecular disulfide bonds. Cartoon representation of kinase domain with N-
1240 lobe colored dark blue/purple and the C-lobe colored light blue/purple. (b) ARK
1241 family member BRSK2, MELK, and MARK2/3 crystal structures demonstrate the
1242 ability to form asymetric dimers bringing T + 2 cys into proximity. Crystal
1243 structures for MARK2, and MELK both contain intermolecular disulfide bonds

1244 between T + 2 cys (Marx et al. 2010; Marx et al. 2006; Murphy et al. 2007; Cao
1245 et al. 2013).

a

b

PKA numbering	157	158	159	160	161	162	163	164	165	166
Alanine	1.7	3.0	6.7	7.0	2.6	0.1	6.1	0.5	2.2	0.6
Cysteine	10.4	0.1	0.6	3.4	0.8	2.2	1.8	0.7	2.1	0.4
Aspartic Acid		0.0	7.2	0.3	3.4	0.0	0.0	0.0	0.0	91.5
Glutamic Acid	0.0	5.9	10.8	2.0	1.9	0.0	0.6	0.1	0.1	0.1
Phenylalanine	0.3	0.0	0.8	1.4	0.8	9.7	1.7	0.4	0.5	0.1
Glycine	0.1	0.4	3.4	1.2	31.1	0.0	0.3	0.0	6.6	0.2
Histidine	0.0	78.2	1.8	10.9	5.6	0.3	0.1	88.8	0.6	0.4
Isoleucine	12.9	0.1	0.4	1.1	0.2	44.1	35.9	0.0	0.0	0.1
Lysine	0.0	2.1	8.9	17.5	10.8	1.7	0.0	0.0	1.8	0.1
Leucine	62.1	0.1	1.0	9.8	0.4	10.8	14.1	0.7	2.7	0.1
Methionine	6.0	0.0	0.3	5.6	1.1	1.3	3.9	0.1	0.4	0.1
Asparagine	0.0	1.8	4.7	11.5	17.3	0.0	0.0	0.1	0.7	3.5
Proline	0.0	0.0	3.2	0.5	2.1	0.0	0.6	0.0	0.0	0.0
Glutamine	0.0	0.7	6.3	7.8	3.6	0.3	0.0	0.0	0.2	0.1
Arginine	0.0	2.2	6.8	9.9	8.5	0.3	0.3	0.2	77.5	0.4
Serine	0.7	3.0	30.3	1.9	4.8	0.7	1.1	0.0	1.4	0.9
Threonine	0.1	0.1	3.8	0.4	0.9	0.5	1.9	0.1	1.7	0.2
Valine	4.7	0.3	0.6	2.1	0.2	21.0	30.4	0.2	0.0	0.4
Tryptophan	0.0	0.2	0.0	0.0	2.0	0.0	0.0	0.0	0.0	0.0
Tyrosine	0.0	0.8	0.7	1.1	0.6	5.9	0.3	7.1	0.5	0.2
-	1.0	1.0	1.5	4.7	1.4	1.0	0.9	0.9	0.9	0.9

PKA numbering	184	185	186	187	188	189	190	191	192	193	–	–	194	195	196	197	198	199	200	201	202	203	204	205	206	207	208
Alanine	0.6	0.4	1.8	1.7	51.4	6.4	6.2	5.0	3.3	3.8	4.2	4.8	5.6	7.8	3.5	3.3	3.1	8.6	4.6	0.5	6.2	7.3	0.1	7.5	65.5	0.3	0.1
Cysteine	0.4	0.7	0.5	1.0	8.2	3.1	0.6	0.6	0.4	0.4	0.7	1.1	0.8	1.7	0.8	0.5	0.8	17.6	1.3	1.3	0.3	2.4	0.2	1.3	1.0	0.0	0.2
Aspartic Acid	91.1	0.0	1.9	0.7	0.4	0.5	6.9	1.7	9.2	13.4	5.5	5.3	4.6	2.8	4.6	2.6	2.1	1.0	0.9	1.5	0.8	5.8	0.1	0.4	0.5	0.2	2.9
Glutamic Acid	0.1	0.0	1.8	0.2	0.2	2.7	8.9	3.1	7.4	7.6	7.6	6.8	6.1	1.1	4.7	3.9	4.2	1.6	0.5	0.8	1.3	8.0	0.0	0.1	0.0	0.6	90.1
Phenylalanine	0.1	81.5	0.1	10.2	1.4	1.1	5.9	8.7	1.0	1.2	0.6	1.5	3.9	3.0	1.4	0.3	13.0	1.2	0.7	2.3	0.9	5.6	8.4	0.6	0.0	0.0	0.1
Glycine	3.4	0.1	89.7	0.1	2.3	3.1	2.4	2.6	6.5	6.0	11.2	4.2	2.2	2.2	6.4	4.8	3.4	5.2	56.9	0.1	0.3	5.1	0.0	0.0	1.3	0.0	0.1
Histidine	0.1	0.2	0.2	0.9	0.1	1.2	3.1	1.3	4.8	4.0	2.8	1.3	3.0	3.3	2.8	2.4	1.4	1.5	0.2	0.2	0.5	2.7	0.7	0.1	0.3	0.0	0.0
Isoleucine	0.0	0.2	0.0	6.2	0.8	2.0	7.2	11.3	3.2	1.6	4.4	2.3	1.7	2.4	0.7	1.3	3.7	7.5	1.2	2.6	4.3	0.7	0.1	7.8	0.0	3.2	0.0
Lysine	0.2	0.1	0.0	0.2	0.5	18.3	7.1	5.8	7.0	3.3	6.0	4.4	10.5	4.6	10.4	2.4	3.3	1.1	5.9	0.4	2.4	6.6	0.0	1.5	0.0	0.3	0.0
Leucine	0.1	9.8	0.1	47.3	1.3	2.0	7.0	17.7	3.6	3.6	2.2	2.0	7.1	13.5	1.5	1.1	11.2	3.6	1.2	4.8	12.5	3.7	0.6	11.5	0.2	1.7	0.3
Methionine	0.3	0.6	0.0	5.1	0.7	0.9	2.5	4.7	2.3	0.7	2.4	1.0	2.9	5.8	1.6	0.4	3.0	0.8	0.6	0.5	0.7	1.4	0.0	30.0	0.0	0.2	0.0
Asparagine	1.0	0.2	0.8	1.2	0.4	3.9	1.5	1.7	4.8	4.1	5.8	3.2	3.3	2.5	7.7	4.9	2.8	1.0	0.5	2.2	0.4	5.0	0.1	0.1	0.0	0.3	2.4
Proline	0.0	0.5	0.0	0.5	0.2	0.3	2.7	2.0	5.3	6.0	1.8	3.9	6.4	1.6	0.7	3.7	2.8	1.1	0.3	0.2	42.2	4.5	0.0	0.0	9.2	88.8	0.0
Glutamine	0.0	0.0	0.0	0.7	0.1	1.5	7.8	1.8	4.3	3.4	4.3	3.0	4.1	2.4	3.0	3.2	3.7	1.4	2.9	0.1	1.1	2.9	0.1	1.0	0.0	0.1	0.3
Arginine	0.1	0.1	0.3	0.6	0.1	28.4	5.3	2.1	5.2	2.1	6.3	3.9	8.4	10.5	4.8	1.6	6.2	2.3	2.6	1.5	15.1	10.4	0.3	20.2	0.3	0.2	0.3
Serine	1.0	0.2	1.7	9.9	25.4	4.9	4.1	3.1	7.6	10.7	3.9	5.7	4.9	5.1	11.9	14.4	4.7	3.7	3.0	15.8	1.8	2.4	0.1	1.9	18.1	0.3	0.1
Threonine	0.4	0.1	0.0	2.0	2.5	9.5	2.9	4.1	4.9	6.0	5.7	7.6	8.1	8.6	18.8	27.6	2.6	4.7	1.3	59.0	0.8	1.5	0.2	6.3	0.3	0.2	0.1
Valine	0.0	1.0	0.0	7.4	2.1	5.2	5.8	10.1	2.8	2.4	3.4	3.4	6.7	2.2	2.1	3.4	7.7	29.7	8.4	1.5	3.1	0.6	0.1	5.5	0.0	0.7	0.1
Tryptophan	0.0	1.3	0.0	1.2	0.3	0.1	1.2	0.5	0.1	0.1	0.2	0.1	0.1	0.5	1.4	0.0	0.6	0.1	0.3	0.7	0.0	10.8	22.4	0.1		0.3	0.0
Tyrosine	0.3	2.6	0.0	0.9	0.5	0.6	3.4	4.9	4.2	0.5	5.4	3.4	1.9	7.1	3.7	0.2	9.5	1.2	1.0	0.3	1.3	9.3	63.3	1.0	0.0	0.0	0.2
-	0.7	0.7	0.8	1.9	1.0	4.5	7.7	7.3	12.3	19.0	15.8	30.8	7.8	11.5	7.5	17.8	10.4	5.2	5.8	3.8	3.9	3.5	3.2	3.1	3.1	2.7	2.6

BRSK Cys

EPK Motif

Supplementary Figure 1: Phylogenetic analysis of BRSK and the ARK family. (a) Phylogenetic analysis of the ARK family reveals that the closest relative of BRSK kinases is AMPK. The number of cysteines in the kinase domain of BRSKs increases relative to AMPK. (b) Sequence alignment and relative amino acid composition of the activation segment of ePKs (top). Data is presented as HMM (hidden Markov models) Sequence Logos. Table (bottom) depicts the frequency of an amino acid at each position along the Catalytic and T-Loop. Key Cys residues are highlighted in orange; residues highly conserved in ePK canonical kinase motifs are highlighted in blue.

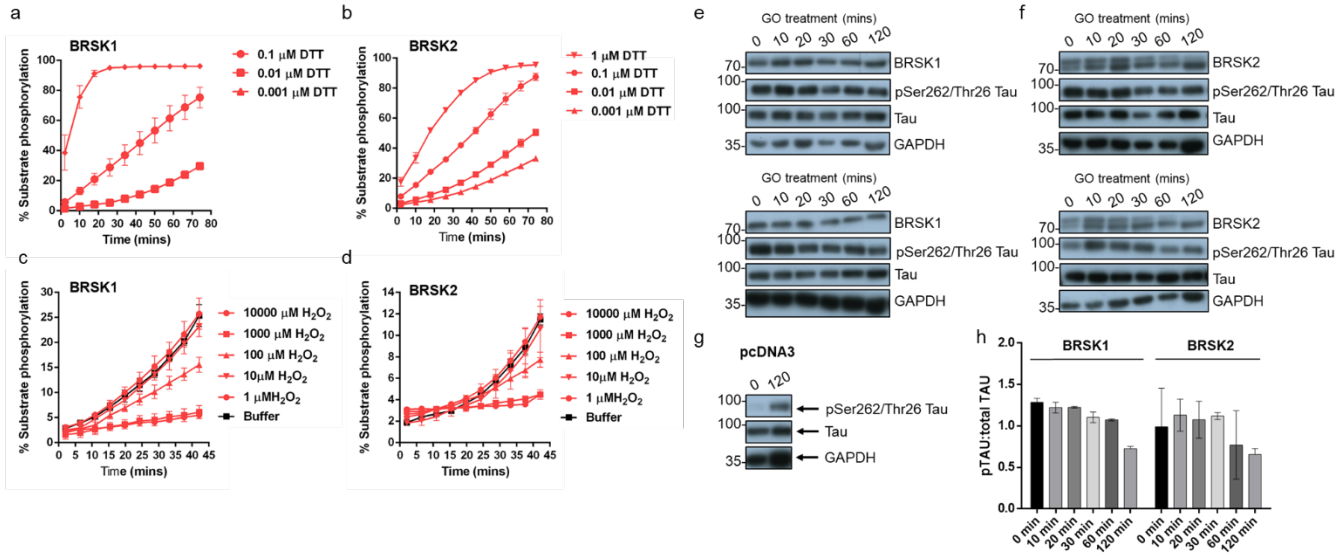

Supplementary Figure 2: Redox regulation of BRSK1 & 2. (a-d) Real-time phosphorylation of fluorescent AMARA peptide by full length BRSK1 and 2 (200 ng). BRSK proteins were incubated with buffer or the indicated concentrations of DTT or H_2O_2. Rates of BRSK activity were calculated as pmol per min phosphate incorporation and are presented in Fig 1. Data shown here is a subset of the conditions shown in Fig 1 (mean and SD from three repeats). (e-h) Time dependent loss of pTAU by incubation of HEK-293T cells with 2U/ml glucose oxidase (GO). Cells were transiently co-transfected with EGFP-Tau and either (e) BRSK1, (f) BRSK2 or (g) empty vector (pcDNA3). Data shown is WB analysis from 2 independent repeats. (h) pTau:Tau signals calculated with ImageJ. Data shown is mean and SD, calculated from (e) and (f).

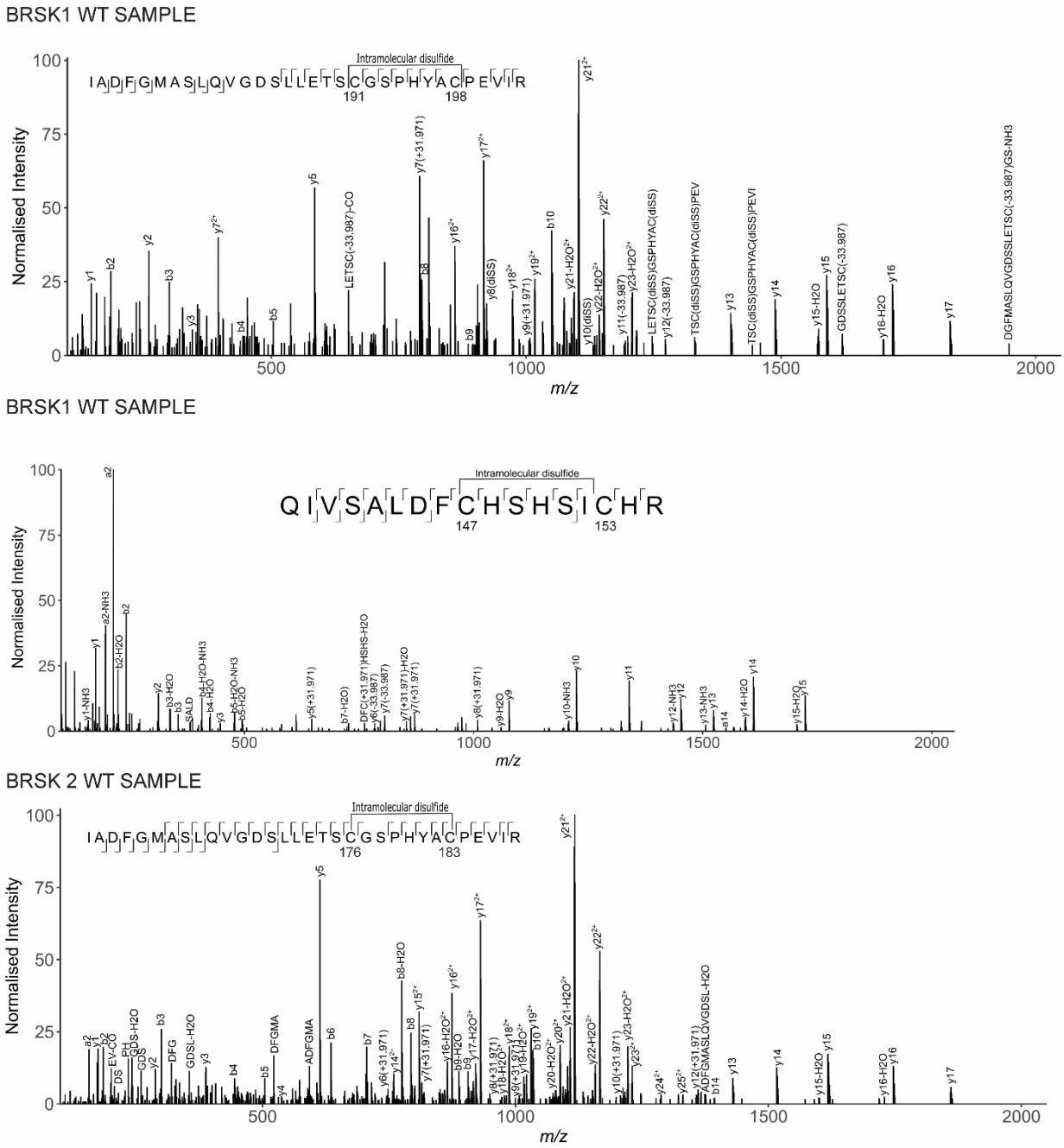

Supplementary Figure 3: LC-MS/MS Analysis of BRSK1/2 catalytic domains. LC-MS/MS reveals intramolecular disulfide bonds in the kinase domains of BRSK1 and 2 purified from *E. coli*.

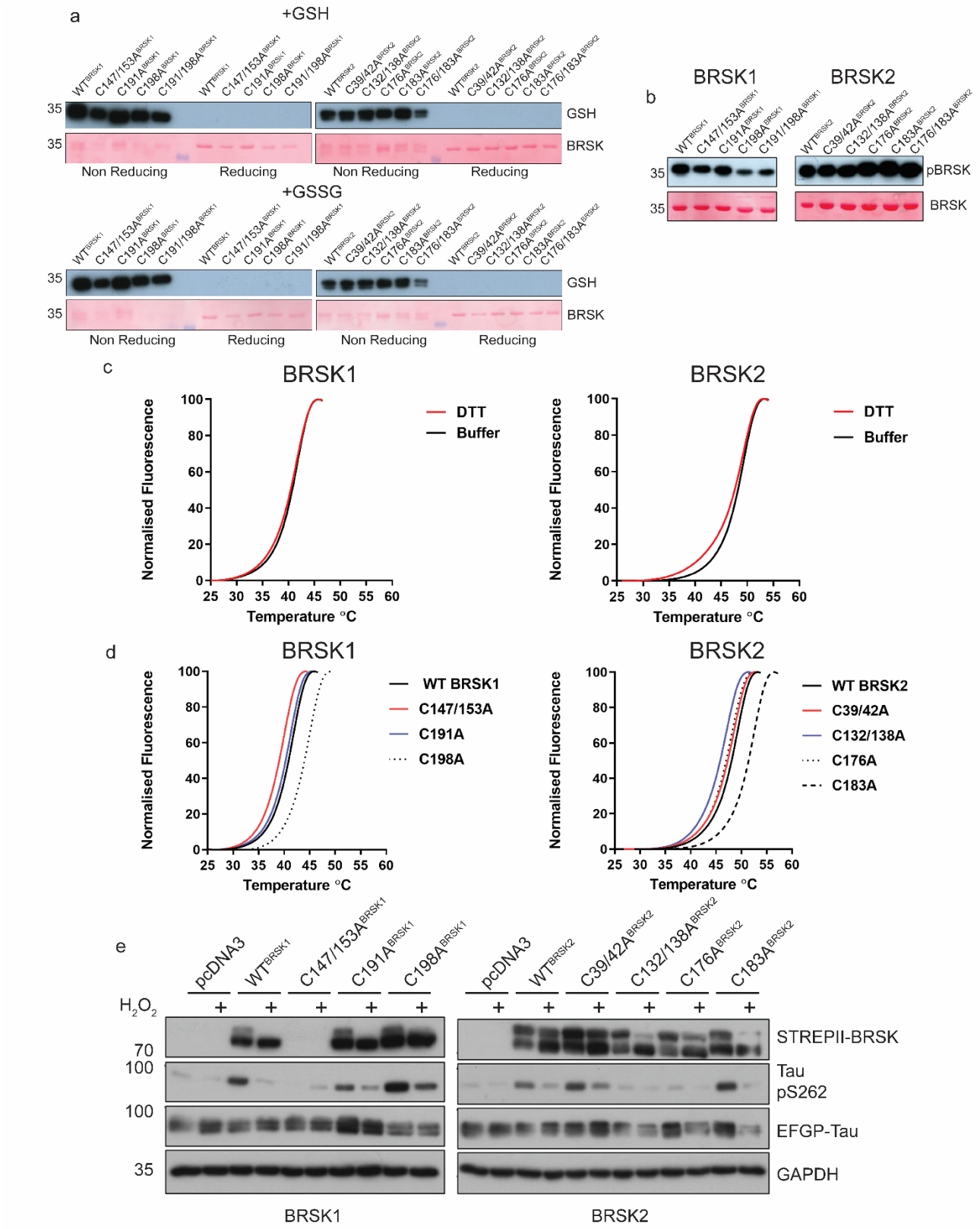
a
+GSH
WT BRSK1
C147/153A BRSK1
C191A BRSK1
C198A BRSK1
C191/198A BRSK1
WT BRSK2
C39/42A BRSK2
C132/138A BRSK2
C176A BRSK2
C183A BRSK2
C176/183A BRSK2
35
GSH
BRSK
Non Reducing
Reducing
+GSSG
b
BRSK1
BRSK2
pBRSK
c
BRSK1
BRSK2
Normalised Fluorescence
Temperature °C
DTT
Buffer
d
WT BRSK1
C147/153A
C191A
C198A
WT BRSK2
C39/42A
C132/138A
C176A
C183A
e
pcDNA3
H2O2
STREPII-BRSK
Tau pS262
EFGP-Tau
GAPDH
70
100
BRSK1
BRSK2

1265

1266 Supplementary Figure 4: Biochemical analysis of BRSK Cys-to Ala mutants. (a)
1267 Immunoblot of in vitro glutathionylation of BRSK kinase domains. (b) Immunoblot
1268 showing LKB1-dependent phosphorylation of BRSK kinase domain proteins. (c)
1269 Thermal denaturation curves of BRSK catalytic domain proteins in the presence
1270 or absence of 10 mM DTT. (d) Thermal denaturation curves of BRSK catalytic
1271 domain cysteine to alanine mutants. (e) Representative immunoblot of EGFP-
1272 Tau co-expressed with full length, WT and Cys-to-Ala mutants of BRSK1 and
1273 BRSK2. Transiently transfected HEK-293T cells were treated with or without 10
1274 mM H_2O_2 for 10 mins.

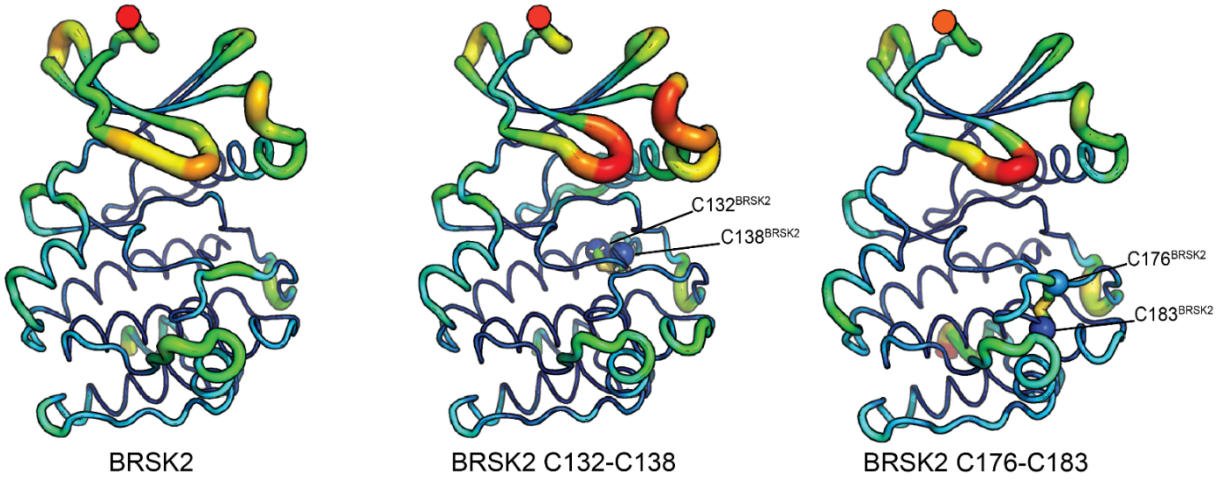

1275 Supplementary Figure 5: Molecular Dynamics Simulations of intramolecular disulfide
1276 bonds. Simulations incorporating disulfide bonds identified in MS/MS
1277 experiments. RMSF was calculated based on three 100 ns GROMACS molecular
1278 dynamics simulations. Higher mobility is indicated by warmer colors and
1279 thickness of representation.
1280
1281
1282

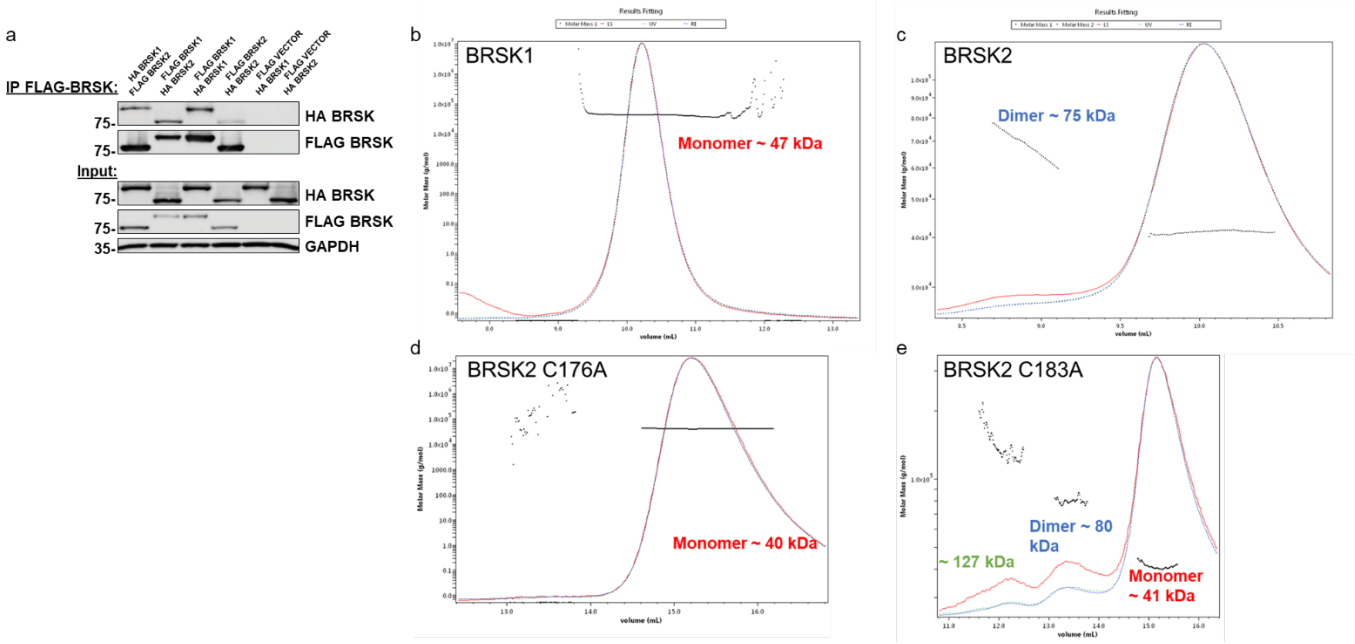

Supplementary Figure 6: Evidence for limited BRKS dimer species. (a) Co-immunoprecipitation of HA-BRSK1/2 with immunoprecipitated FLAG-BRSK1/2 expressed in HEK-293T cells. SEC-MALS analysis of WT (b) BRSK1 and (c) 2, and (d) C176A and (e) C183A BRSK2 kinase domains in solution, performed in the absence of reducing agents.

1137

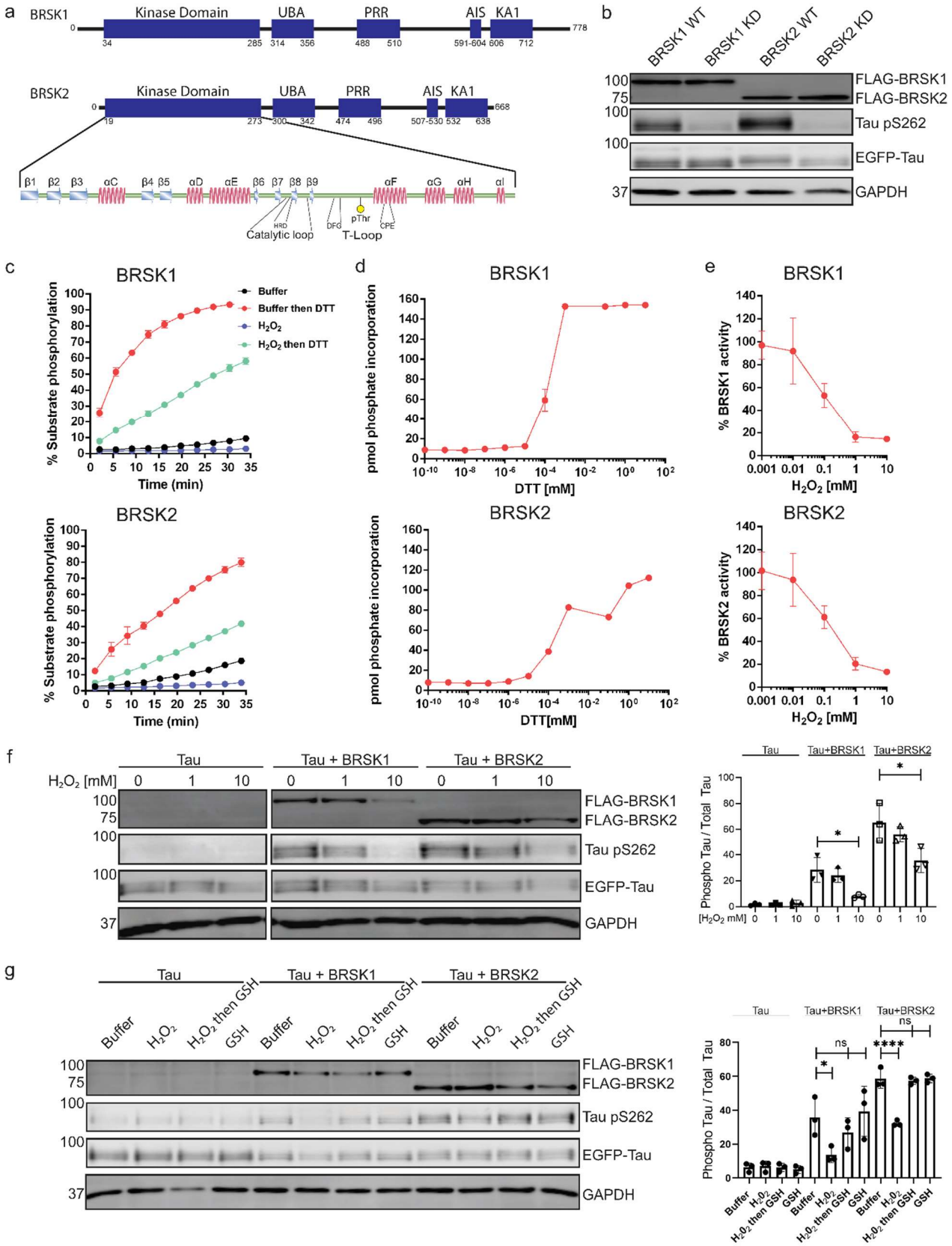
a
BRSK1
Kinase Domain
UBA
PRR
AIS
KA1
BRSK2
Catalytic loop
T-Loop
b
BRSK1 WT
BRSK1 KD
BRSK2 WT
BRSK2 KD
FLAG-BRSK1
FLAG-BRSK2
Tau pS262
EGFP-Tau
GAPDH
c
BRSK1
Buffer
Buffer then DTT
H2O2
H2O2 then DTT
% Substrate phosphorylation
Time (min)
BRSK2
d
pmol phosphate incorporation
DTT [mM]
e
% BRSK1 activity
% BRSK2 activity
H2O2 [mM]
f
Tau
Tau + BRSK1
Tau + BRSK2
H2O2 [mM]
Phospho Tau / Total Tau
g
Buffer
H2O2
H2O2 then GSH
GSH
ns
****

1138 Figure 1: BRSK1/2 are redox sensitive. (a) Schematic representation of BRSK domain
1139 architecture, including Kinase domain, Ubiquitin Associated (UBA) domain,
1140 Proline-Rich Region (PRR), Kinase Associated Domain(KA1), and Autoinhibitory
1141 Sequence (AIS). (b) Immunoblotting showing BRSK dependent phosphorylation
1142 of Tau at Ser262 (pS262), from lysates of HEK-293T cells overexpressing full-
1143 length FLAG-BRSK1 or 2 (wild type [WT] or kinase dead [KD]) and EGFP-Tau.
1144 (c) Real time phosphorylation of fluorescent AMARA peptide by full length
1145 BRSK1 and 2 (200 ng) purified from Sf21 cells. BRSK proteins were incubated
1146 with buffer or 1 mM H_2O_2 for 10 mins, reactions were then initiated with the
1147 addition of ATP and peptide substrate in the presence (where indicated) of 10
1148 mM DTT. Dose response curves for (d) DTT and (e) H_2O_2 with 200 ng full-length
1149 BRSK1 and BRSK2. All kinases assays are shown as mean and SD of three
1150 experiments. (f) Immunoblott (left) of pS262 in transiently co-transfected HEK-
1151 293T cells incubated with the indicated concentration of H_2O_2 for 10 mins. Signal
1152 density for phospho Tau S262 and total Tau (GFP) was obtained using
1153 ImageStudio software (Licor) and results from at least 3 biological replicates
1154 were anaylzed with Graphpad Prism software using one way anova to determine
1155 significance. Data shown is mean and SE. (g) Representative immunoblot (left)
1156 of transiently co-transfected HEK-293T cells treated with 10 mM H_2O_2 for 10
1157 mins before the addition of 20 mM GSH. Whole cell lysates were harvested after
1158 a further 15 mins. Normalized densitometry of Tau pS262 signal (right) was
1159 calculated from 3 independent experiments. Data shown is mean and SD. * = $P < 0.05$, **= $P < 0.01$, ***= $P < 0.001$.

1161

a

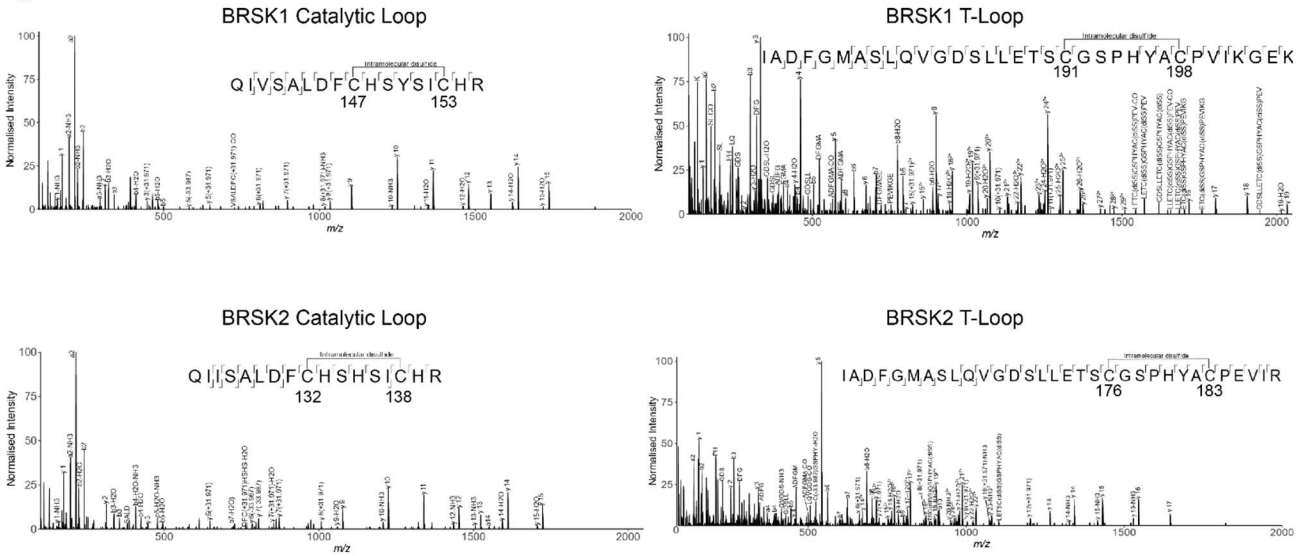
BRSK1 Catalytic Loop
Q I V S A L D F C H S Y S I C H R
147
153
BRSK1 T-Loop
I A D F G M A S L Q V G D S L L E T S C G S P H Y A C P V I K G E K
191
198
BRSK2 Catalytic Loop
Q I I S A L D F C H S H S I C H R
132
138
BRSK2 T-Loop
I A D F G M A S L Q V G D S L L E T S C G S P H Y A C P E V I R
176
183
Normalised Intensity
m/z

b

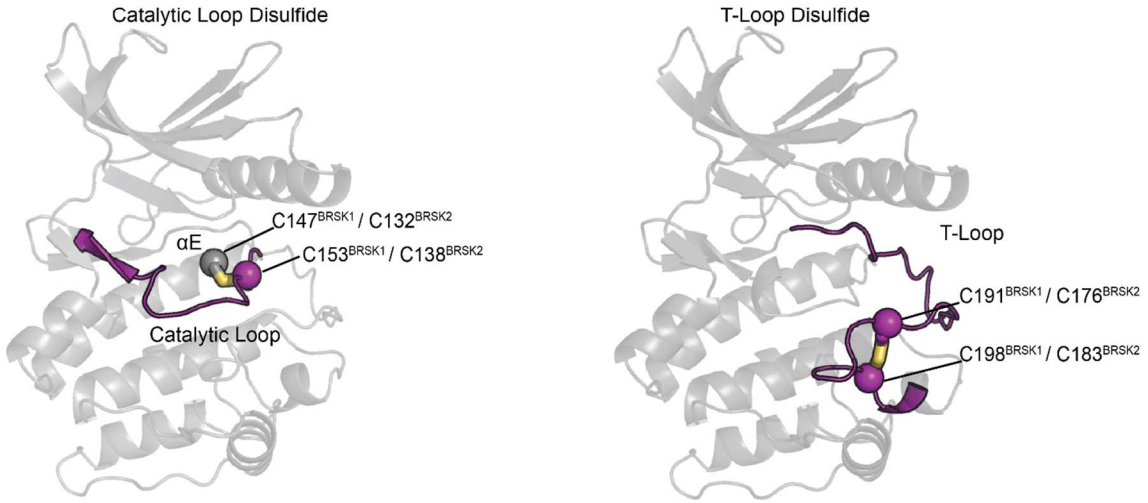
Catalytic Loop Disulfide
αE
C147BRSK1 / C132BRSK2
C153BRSK1 / C138BRSK2
Catalytic Loop
T-Loop Disulfide
T-Loop
C191BRSK1 / C176BRSK2
C198BRSK1 / C183BRSK2

c

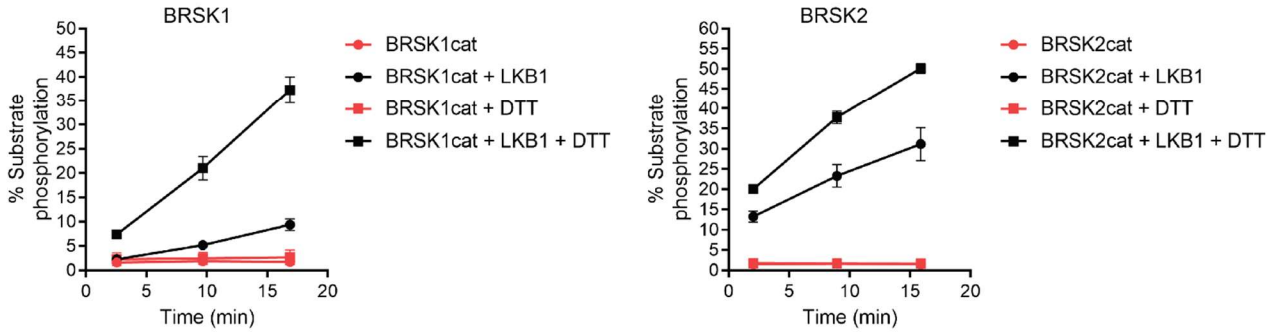
BRSK1
% Substrate phosphorylation
Time (min)
BRSK1cat
BRSK1cat + LKB1
BRSK1cat + DTT
BRSK1cat + LKB1 + DTT
BRSK2
BRSK2cat
BRSK2cat + LKB1
BRSK2cat + DTT
BRSK2cat + LKB1 + DTT

1162 Figure 2: Intramolecular disulfide bonds form in the kinase domains of BRSK1 and 2. (a)
1163 Full length BRSK1 and 2 were affinity-purified from HEK-293T cells and
1164 subjected to LC-MS/MS analysis. LC-MS/MS spectrum mapping revealed
1165 disulfide bridges formation between $C147^{BRSK1}$ - $C153^{BRSK1}$, $C191^{BRSK1}$ -
1166 $C198^{BRSK1}$, $C132^{BRSK2}$ - $C138^{BRSK2}$, and $C176^{BRSK2}$ - $C183^{BRSK2}$. Peptide
1167 coverage was 74 and 78 % for BRSK1 and BRSK2 respectively. (b) Alphafold
1168 structures demonstrating the location of disulfide bonds within the kinase
1169 domains of BRSK1 and BRSK2. (c) Real time phosphorylation of fluorescent
1170 AMARA peptide by the kinase domains of BRSK1 and 2 (100 ng) purified from
1171 *E.coli* . BRSK1 (29-358) and BRSK2 (14-341) were activated by incubation with
1172 LKB1 and assayed in the presence or absence of 1 mM DTT.

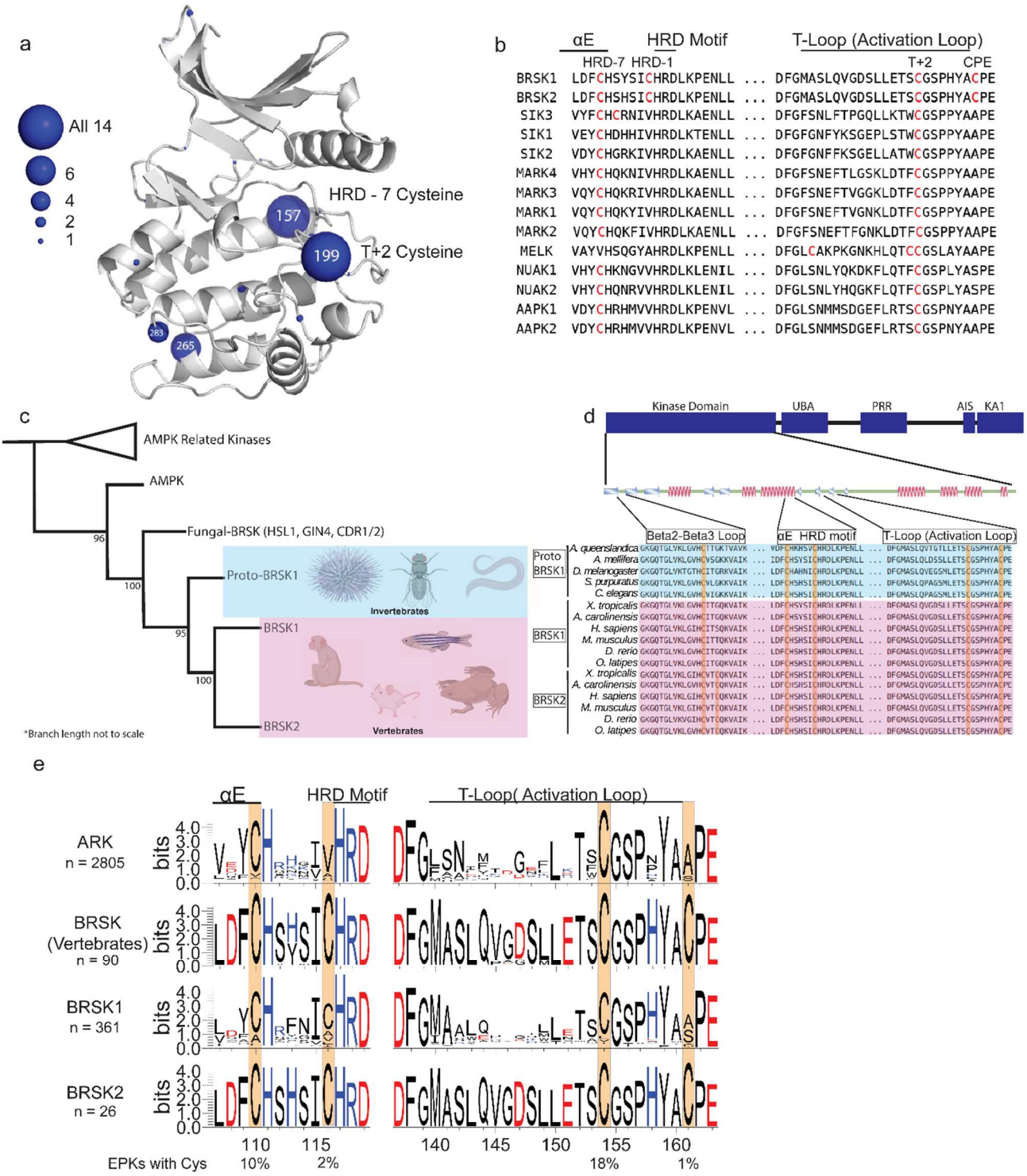

Figure 3: Cysteine pairs are highly conserved within the activation segments of BRSKs. (a) Mapping of Cys residues (spheres) in the kinase domains of human ARK family members. Numbers represent the corresponding amino acid position in

PKA. Sphere size is proportional to the number of ARKs that contain a Cys at a specific site. (b) Activation segment sequence alignment of the 14 human ARKs. (c) Phylogenetic analysis showing divergence and grouping of BRSKs sub-families in different taxonomic groups. Bootstrap values are included for each clade. (d) Sequence alignment of the kinase domains of invertebrate and vertebrate BRSKs. (e) Analysis of relative amino acid conservation in ARKs and BRSKs, centered on the HRD containing catalytic loop, and the T-loop (between the DFG and APE motifs). Data is presented as HMM (hidden Markov models) Sequence Logos. The % of ePKs that possess a specific Cys is shown at the bottom.

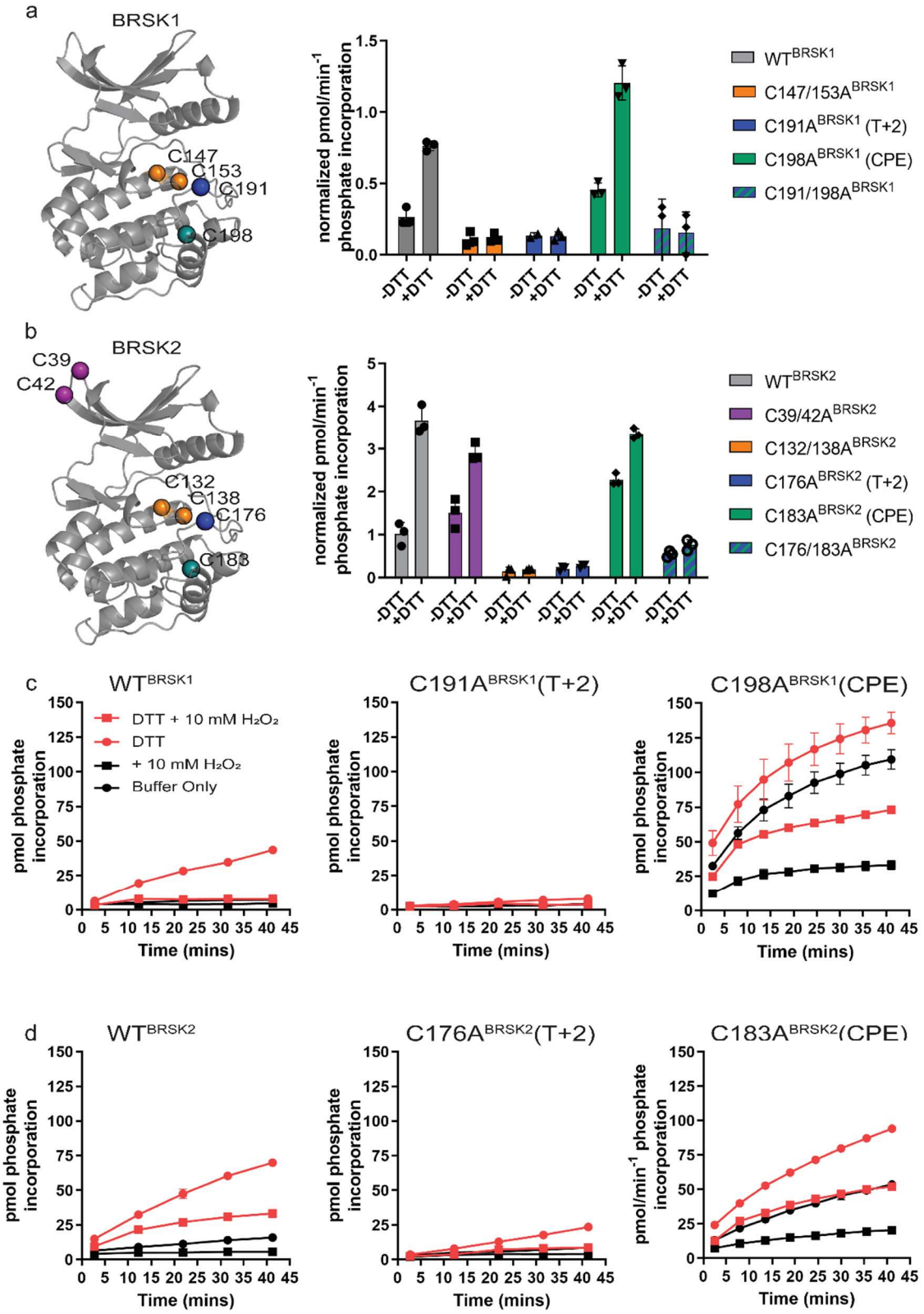
a
BRSK1
C147
C153
C191
C198
normalized pmol/min-1 phosphate incorporation
WTBRSK1
C147/153ABRSK1
C191ABRSK1 (T+2)
C198ABRSK1 (CPE)
C191/198ABRSK1
-DTT
+DTT
b
BRSK2
C39
C42
C132
C138
C176
C183
WTBRSK2
C39/42ABRSK2
C132/138ABRSK2
C176ABRSK2 (T+2)
C183ABRSK2 (CPE)
C176/183ABRSK2
c
WTBRSK1
C191ABRSK1(T+2)
C198ABRSK1(CPE)
DTT + 10 mM H2O2
DTT
+ 10 mM H2O2
Buffer Only
pmol phosphate incorporation
Time (mins)
d
WTBRSK2
C176ABRSK2(T+2)
C183ABRSK2(CPE)
pmol/min-1 phosphate incorporation

1187

1188

1189 Figure 4: Cysteine residues within the kinase domain fine-tune BRSK activity. In vitro
1190 kinase assays (right panels) showing normalized rates of peptide
1191 phosphorylation by WT and Cys-to-Ala variants of (a) BRSK1 and (b) BRSK2.
1192 100 ng of LKB1 activated BRSK kinase domain was assayed in the presence or
1193 absence of 1 mM DTT. The positions of mutated Cys residues are modelled on
1194 the kinase domain as coloured spheres (left panel). Real time in vitro assays
1195 using (c) 50 ng BRSK1 and (d) 20 ng BRSK2. LKB1-activated BRSK proteins
1196 were incubated on ice in the presence or absence of 250 μM DTT for 30 mins.
1197 Assays were initiated by the addition of ATP and fluorescent peptide substrate in
1198 the presence or absence of 1 mM H_2O_2. All data is mean and SD of 3
1199 experiments and activities are normalized to LKB1-phosphorylated BRSK signal
1200 (Supp Fig 4 b).
1201

1202

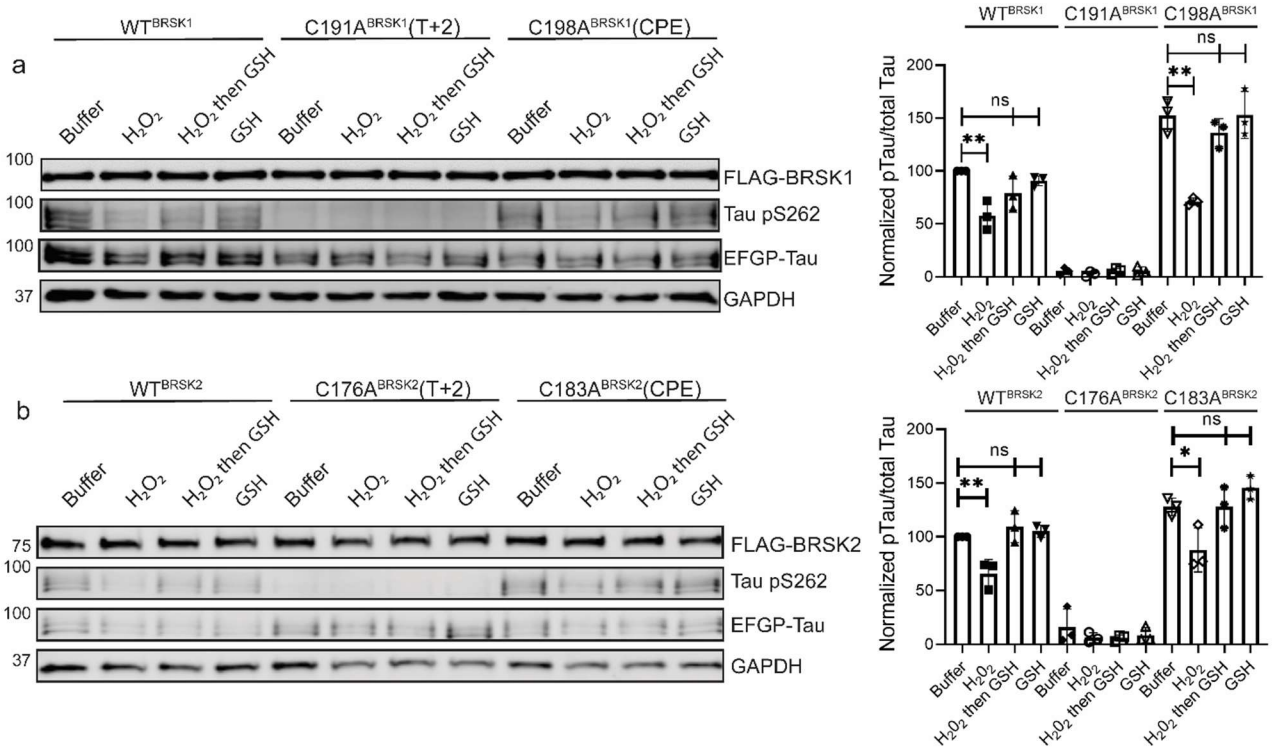

1203

1204 Figure 5: Impact of T-Loop and CPE Cys-to-Ala mutations on BRSK redox sensitivity in
1205 a cellular EGFP-Tau HEK-293T co-expression system. Representative
1206 immunoblot of EGFP-Tau co-expressed with WT and Cys-to-Ala mutants of (a)
1207 BRSK1 and (b) BRSK2 (left panels). Transiently transfected HEK-293T cells
1208 were treated with or without 10 mM H_2O_2 for 10 mins before the addition of 20

mM GSH. Whole cell lysates were harvested after a further 15 mins. Signal density for phospho Tau S262 and total Tau (GFP) was obtained using ImageStudio software (Licor) and results from at least 3 biological replicates were anaylzed with Graphpad Prism software using one way anova to determine significance (right panels). Data shown is mean and SE. All values are normalized to Tau pS262 signals from control (buffer only treatment) WT BRSK and Tau co-transfections. Data shown is mean and SD. * = P < 0.05, **= P < 0.01, ***= P < 0.001.

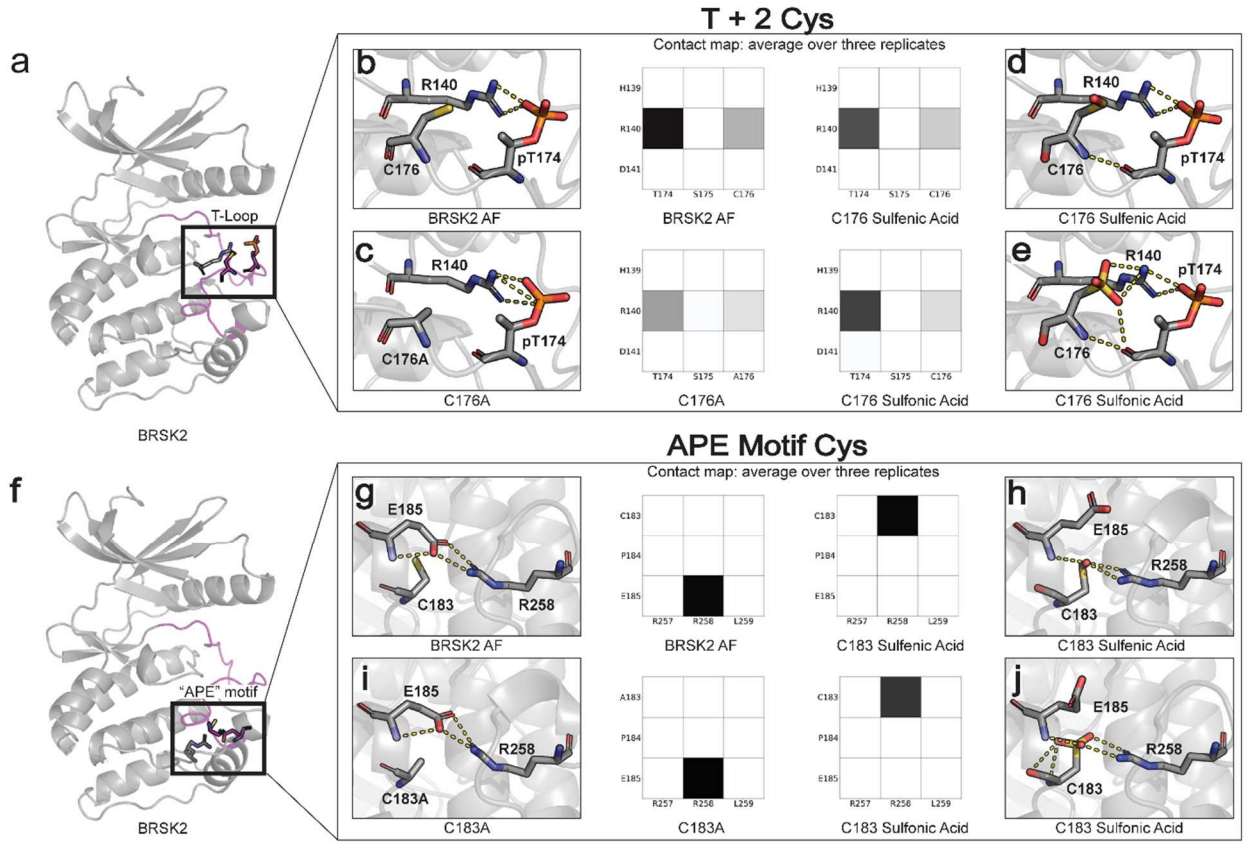

Figure 6: Oxidative cysteine modifications alter critical structural interactions required for BRSK allosteric regulation. Three replicates of 100 ns GROMACS molecular dynamics simulations were performed to evaluate the effects of cysteine mutation and oxidation. Salt bridge disruption was analyzed by generating contact maps representing the percentage of the simulation time in which residues were within appropriate distance (3 Angstroms). (a) T+2 Cys is located in proximity to the activation loop threonine in the T loop. (b-e) Evaluation of pT174-R140 salt bridge formation in wild type, C176A, and oxidized C176 BRSK2. (f) Location of CPE salt bridge within BRSK2. (g-j) Evaluation of E185-R258 salt bridge formation in wild type, C183A, and oxidized C183 BRSK2.

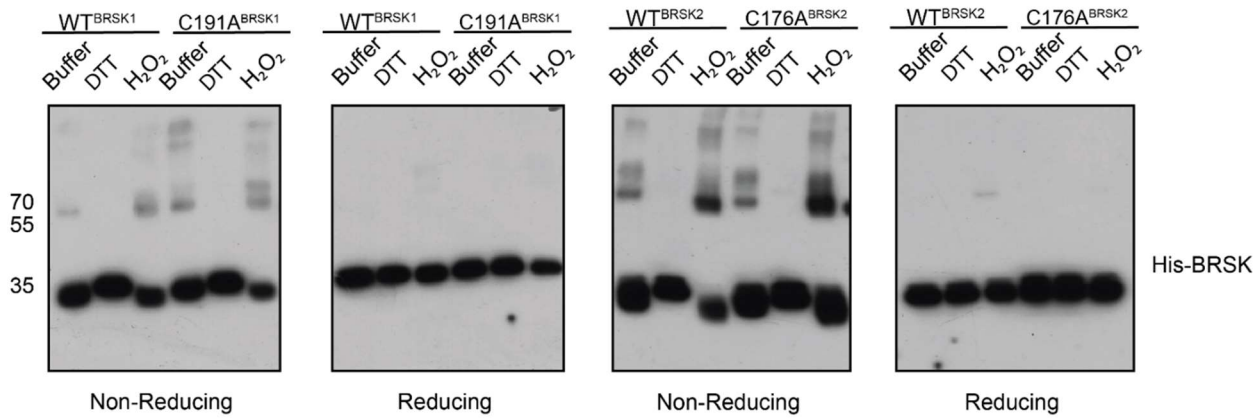

Figure 7: BRSK1/2 form limited disulfide-mediated multimers. Western blot analysis of BRSK1/2 kinase domain purified from *E. coli* and incubated with buffer, H_2O_2, or DTT and subjected to non-reducing or reducing PAGE to evalute the formation of intramolecular disulfide bonds.

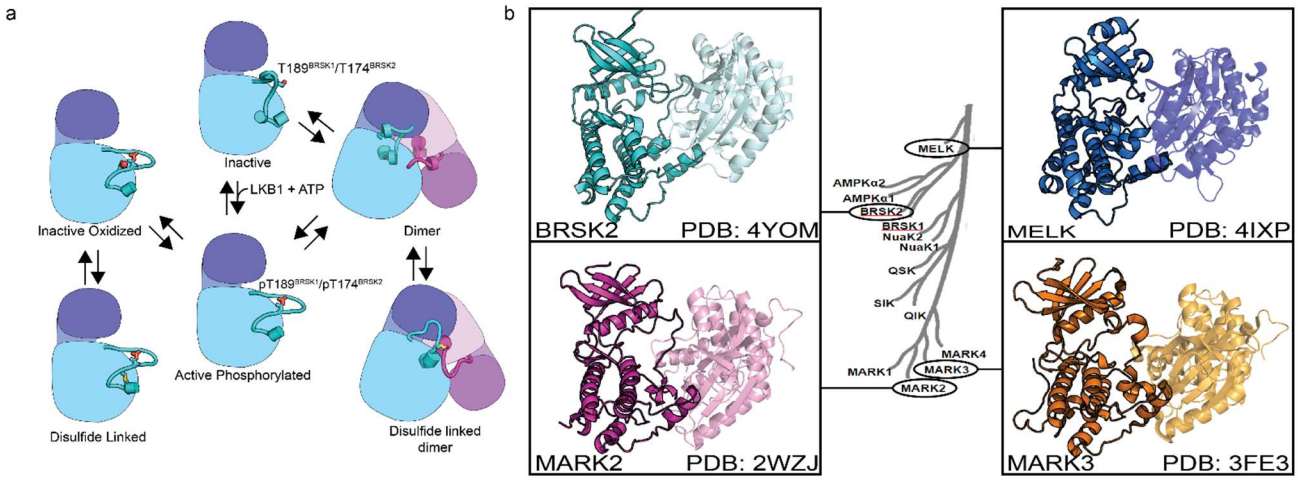

Figure 8: (a) Model of BRSK1/2 regulation. Schematic diagram demonstrating ways in which residues within BRSK kinases permit fine-tuning of catalytic activity through a variety of oxidative modifications, potentially including inter and intramolecular disulfide bonds. Cartoon representation of kinase domain with N-lobe colored dark blue/purple and the C-lobe colored light blue/purple. (b) ARK family member BRSK2, MELK, and MARK2/3 crystal structures demonstrate the ability to form asymetric dimers bringing T + 2 cys into proximity. Crystal structures for MARK2, and MELK both contain intermolecular disulfide bonds

1244 between T + 2 cys (Marx et al. 2010; Marx et al. 2006; Murphy et al. 2007; Cao
1245 et al. 2013).